CHALMERS
UNIVERSITY OF TECHNOLOGY

Bearing Load Measurement System

To verify whether the FBG sensors can be used to measure axial strain on rotor bearing

Master's thesis in Mobility Engineering

KAUSTUBH GIRIDHAR SETLOOR
KUSHAL LAKSHMANA GOWDA

Department Of Industrial and Material Sciences

CHALMERS UNIVERSITY OF TECHNOLOGY
Gothenburg, Sweden 2024
www.chalmers.se

Master's thesis 2024

BEARING LOAD MEASUREMENT SYSTEM

To verify whether the FBG sensors can be used to measure axial strain on rotor bearing

KAUSTUBH GIRIDHAR SETLOOR
KUSHAL LAKSHMANA GOWDA

CHALMERS
UNIVERSITY OF TECHNOLOGY

Department of Industrial and Material Sciences
Division of Product Development
Chalmers University of Technology
Gothenburg, Sweden 2024

Bearing Load Measurement System
To verify whether the FBG sensors can be used to measure axial strain on rotor bearing.

KAUSTUBH G SETLOOR
KUSHAL LAKSHAMANA GOWDA

Supervisor: Sebastian Paling, Volvo Car Corporation
Supervisor: Johan Cederlund, Volvo Car Corporation
Examiner: Magnus Evertsson, Industrial and Material Science

Master's Thesis 2024
Department of Industrial and Material Science
Division of Product Development
Chalmers University of Technology
SE-412 96 Gothenburg
Telephone +46 31 772 1000

Abstract

The advancement of sensor technology plays a crucial role in enhancing performance and reliability of mechanical systems. In the world of industrial applications, the accurate monitoring of mechanical components is essential to ensure good operational performance and efficiency with prevention of failures. One promising technology for such monitoring tasks is the Fiber Bragg Grating Sensors (FBG).

This thesis helps us validate and verify the application of Fiber Bragg Grating (FBG) sensors for monitoring axial strain on mechanical ball bearings of an electric motor. It focuses on the effectiveness of the sensors in providing precise strain measurements for improving monitoring technology in mechanical systems. The research research was divided into 4 main tasks: preliminary research, development of python-based interrogator software including a graphical user interface (GUI) for data capture, test setup development for applying axial loads on the bearing and data analysis/-post processing. This research employs Python software for every process involved from collecting the FBG data to post process of the data.

The preliminary research involved an extensive review of existing literature to establish a strong theoretical foundation on sensor technology and its application. A python-based software was developed to interface with the Sentea interrogator for which a user-friendly GUI was designed to capture real-time sensor data for data visualization and export. The test rig setup involved applying axial loads to the rotor shaft of the electric motor using a hydraulic press, with custom-designed components to ensure accurate application of force on the bearings and for accurate measurement. The sensors were installed along the outer-ring of the ball bearings and the tests were conducted under varying load conditions with rotation speed of 600rpm with the use of hand drill. The collected data was processed to calculate strain and stress.

The post-processing involved filtering the data, calculating strain and stress, and analyzing the results through discrete Fourier transforms to understand the dynamic behavior of the bearings under load and the obtained plots and result shows that the axial strain with respect to the load increases linearly with curve fit. Hence, this work concludes that the findings demonstrate the potential of FBG sensors in providing strain measurements, validating for advanced monitoring of mechanical systems. This research offers valuable insights into the use of these sensors for industrial applications, offering a foundation for future studies and technological advancements in this field.

Keywords: Fiber Bragg Grating (FBG), Axial Strain, Deep Grove Ball Bearings, Interrogator, Discrete Fourier Transform, Butterworth Filter

Acknowledgements

This thesis research work was carried out at Volvo Car Corporation in collaboration with Chalmers University of Technology's Industrial and Material Sciences department. We would like to thank our Academic Examiner, Magnus Evertsson for his continued support throughout the period of this Thesis. We would also like to thank our company Supervisor and Co-supervisor from Volvo Cars, Sebastian Paling and Johan Cederlund for sharing their knowledge and their guidance. We are also very thankful for our entire team for making us feel welcomed. We would also like to thank Staffan Jaktling and Roland Petersson for their help during their busy schedule. We also appreciate the help we received from the Mechanics at the workshop. We would like give our thanks to our partner companies Sentea and Sensing 360 for their help. Lastly, we would like to thank Volvo Car Corporation for giving us this wonderful opportunity to work here and gain some professional experience.

Kaustubh Giridhar Setloor, Kushal Lakshmana Gowda, Gothenburg, June 2024

Contents

List of Acronyms **xi**

List of Figures **xii**

List of Tables **xiv**

1 Introduction **1**
1.1 Background . . . 1
1.2 Aim and Objective . . . 2
1.3 Limitations . . . 3

2 Theory **5**
2.1 Mechanical Strain . . . 5
2.2 Fiber Bragg Grating . . . 6
2.2.1 Applications of FBG . . . 7
2.2.2 Advantages of FBG . . . 7
2.3 FBG Interrogation . . . 8
2.3.1 Advantages of WDM . . . 8
2.4 Electric Machines . . . 8
2.5 Bearings . . . 11
2.5.1 Deep Groove Ball Bearings . . . 12
2.5.2 Observable changes in rotor bearings . . . 14

3 Methodology **17**
3.1 Preliminary Research . . . 17
3.2 Python-based Interrogator software . . . 17
3.2.1 Software Interface . . . 17
3.2.1.1 PeakViewer . . . 18
3.2.1.2 API . . . 18
3.2.2 GUI for capturing the FBG sensor data . . . 19
3.3 Test setup development for applying axial strain on bearing . . . 21
3.3.1 Concept planning . . . 22
3.3.2 Design and Manufacturing . . . 22
3.3.3 Test Environment setup . . . 25
3.3.4 FBG sensor installation . . . 29
3.3.5 Experiment . . . 30
3.4 Post processing . . . 31

4 Results **33**
4.1 GUI 33
4.2 Post-processing results 36
4.2.1 Filtered results 37
4.2.2 Discrete fourier transform 39
4.2.3 Relation between Applied Force vs Wavelength shift 43

5 Conclusion **45**

6 Future Scope **47**

Bibliography **I**

A Appendix 1 **III**

List of Acronyms

Below is the list of acronyms that have been used throughout this thesis listed in alphabetical order:

EV	Electric Vehicles
IC	Internal Combustion
FBG	Fiber Bragg Grating
EMI	Electromagnetic Interference
GUI	Graphic User Interface
WDM	Wavelength Division Multiplexing
TDM	Time Division Multiplexing
SDM	Spacial Division Multiplexing
EM	Electric Machine
HEV	Hybrid Electric Vehicles
PMSM	Permanent Magnet Synchronous Machine
API	Application Programming Interface
DE	Driving End
NDE	Non-Driving End
BPF	Ball Passing Frequency
BPFO	Ball Passing Frequency of Outer ring
RPS	Rotations Per Second
RPM	Rotations Per Minute
DFT	Discrete Fourier Transform
FFT	Fast Fourier Transform

List of Figures

1.1 Rotor with ball bearings of ERAD machine 2

2.1 Mechanical strain of a cylinder with tensile force 5
2.2 Structure and functionality of FBG sensor [1] 6
2.3 Illustration of the behavior of Fiber Bragg Gratings [2] 7
2.4 EM for HEVs and EVs(adapted from [3]) 9
2.5 MEP2 ERAD 10
2.6 Rotor and magnet location 10
2.7 Different types of bearings[4] 12
2.8 Schematic structure of ball bearing 13
2.9 Radial force due to Planetary Load Sharing [5] 14
2.10 Axial force due to sun-gear 15
2.11 Unbalanced Magnetic Pull 15

3.1 SENTEA PeakViewer Software Application 18
3.2 Main Menu of the GUI 20
3.3 Visualization of GUI 20
3.4 Top plate 22
3.5 Wheel Hub 23
3.6 Initial design of Bottom plate 23
3.7 New design of the bottom plate 24
3.8 Final Design Setup 24
3.9 Hydraulic Press 25
3.10 Hydraulic Press with electric machine 26
3.11 Sentea Interrogator 27
3.12 Force Transducer 27
3.13 Dewesoft Amplifier and software 28
3.14 Hand drill mount 28
3.15 Tachometer 29
3.16 FBG fiber and sleeve 30
3.17 Sample data 31

4.1 Samples obtained from GUI 34
4.2 Plot obtained from GUI of Peaks vs Timestamp 34
4.3 Fiber status of GUI 35
4.4 Save as CSV format from GUI 35
4.5 Samples after separation 36

4.6 Original data for all the peaks 36
4.7 Original vs filtered data 3000N for fiber1 37
4.8 Original vs filtered data 3000N for fiber2 38
4.9 All peaks for fiber 1(3000N) 39
4.10 FFT for Fiber 1 under an applied load of 3000N 40
4.11 FFT for Fiber 2 under an applied load of 3000N 41
4.12 Force v/s Average peaks for Fiber 1 43
4.13 Force v/s Average peaks of Fiber 2 44

A.1 1000N fiber1 filtered III
A.2 2000N fiber1 filtered IV
A.3 2500N fiber1 filtered V
A.4 4000N fiber1 filtered VI
A.5 5000N fiber1 filtered VII
A.6 500N DE all peaks VIII
A.7 3000N DE selected peaks VIII
A.8 4000N peaks IX
A.9 5000N peaks X

List of Tables

3.1 Technical Specifications of the Sentea Interrogator DM-8120 [6] . . . 27
3.2 Loading conditions 30

4.1 Comparison of RPM values from Tachometer and FFT under different loads 42

1

Introduction

1.1 Background

The drive to move towards going green, releasing emission free vehicles, is now more than ever. The car companies are rapidly shifting their focus on to the Electric vehicles(EVs) from Internal Combustion(IC) engines. In the grand-scheme of the vehicle manufacturing, this concept is relatively new and each day there are plenty of new research and development being done on this aspect of the cars and it has a potential for a big future in car industry[7]. Due to the huge demand for electrical vehicles in the world, there's need to research and tests on smaller components of the machine. Among the many components that needs to tested and measured, rotor bearing stands out quite a bit as it is constantly subjected to loads, even at no speed and no external load, it is under some load due the weight of the rotor. If these components go undetected, it will result in failure of bearing and the repair cost is very high[8]. These measurement are conducted to get a picture of its durability and reliability. It is important to carry these measurement test at a faster pace as the demand for electrical vehicle is not slowing down but also not to compromise on the accuracy of it. These measurement are needed for future simulation purpose.

One such technology where we can do these measurements fast and also accurately is the FBG sensors. There are plenty applications of this sensors such as measuring strain, temperature, health monitoring, vibration, etc. The growth of this fiber technology has been very rapid over the last couple of decades. This technology has been applied in many fields such as medical, industrial, military, aerospace, automotive,etc. There are several advantages of using this type of sensor when compared to the traditional way of using the strain gauge such as small in size, resistance to chemical corrosion,high resolution, but the main important advantage is its immunity to EMI(Electromagnetic Interference)[9]. The Fiber Bragg Optic(FBG) sensors are embedded in the core of the optic fibers and a single strand of fiber can have multiple sensors, and the best possible to way to distinguish between them is by measuring the reflection wavelength for each sensor as the there is periodic variation in refractive index along the length of the fiber[10]. There is also time based measurement where all sensors in the same fiber will have same wavelength and the sensors are distinguished based on the time when they were sampled. In this thesis, our focus is going to be in measuring the forces experienced by the sensor and validating it with force measured from force sensors and to make sure if this technology can be used for future testings.

1.2 Aim and Objective

In this thesis, the FBG sensor fibers were wrapped around the rotor bearing of an electric motor on both drive end and non-drive end. The main aim of this thesis is as follows:

- Develop an in house GUI for the measurement and data storing using python.
- Develop a script that calculates the force experienced by rotor bearings.
- Help develop test methods to evaluate the usage of this sensor for force measurements.
- With the acquired data, perform data analysis and validate the results with the ones from traditional sensors.

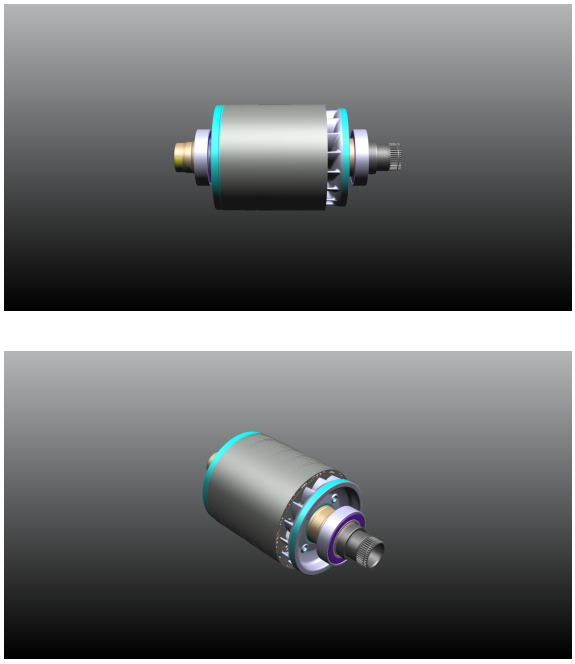

Figure 1.1: Rotor with ball bearings of ERAD machine

1.3 Limitations

Following are the project limitations:

- **Monitoring the loads of just a specific subset of the electric drive train**: The focus is on monitoring the loads on rotor bearings of the electric motor, which means other components of the drive train are not being studied. This limited scope may result in an incomplete understanding of the overall system performance and interactions between different components.
- **Resource constraints limiting the range of real-world testing**: While Volvo Cars provides significant resources, there may still be practical limitations such as time, availability of specific testing equipment, or the number of prototypes available for extensive testing. These constraints might limit the ability to conduct as broad a range of real-world tests as desired, potentially affecting the generalizability of the findings.
- **Inability to fully replicate external conditions**: While the project can consider external factors like temperature, humidity, and vibration, it cannot fully replicate the complex and dynamic real-world conditions. This limitation may affect the accuracy and applicability of the test results, as the controlled environment may not capture all possible variations encountered in actual use.
- **Long-term durability and reliability of FBG sensors**: The Fiber Bragg Grating (FBG) sensors, despite their advantages, may face challenges related to long-term durability and reliability. Factors such as sensor aging, environmental exposure, and the quality of installation could impact their performance over time, potentially affecting the consistency and accuracy of the measurements. This poses a risk to the long-term applicability of FBG sensors for continuous monitoring.

2

Theory

2.1 Mechanical Strain

The most basic definition of a strain is the deformation per unit length experienced by a material due to an applied force. Mathematically, we can define it as change in length over original length of material.

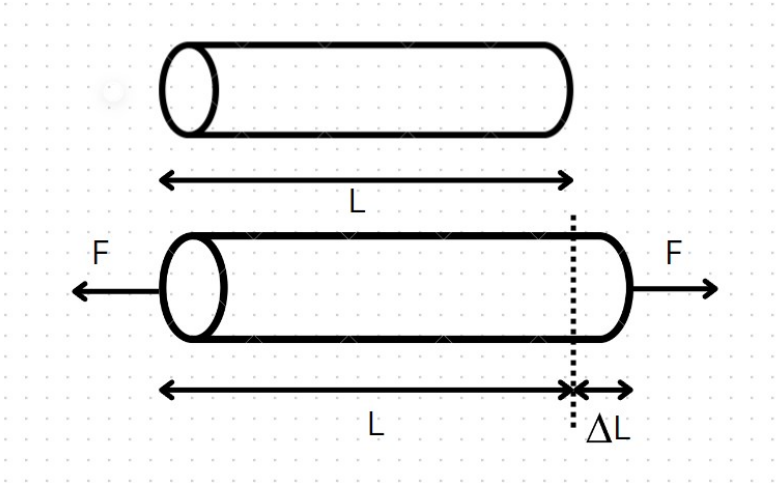

Figure 2.1: Mechanical strain of a cylinder with tensile force

So the strain can be defined as:

$$\epsilon = \frac{\Delta L}{L} \tag{2.1}$$

In this thesis, the FBG fibers that are being used in tests experience both compressive strain and tensile strain. It depends on their position and placement in the electric machine. In rotor bearings, it is important to monitor the stress and strain of the bearing as they are under constant load and this can help us from preventing failures and check on the bearings longevity.

2.2 Fiber Bragg Grating

Fiber Bragg Grating are specialized gratings that are integrated within the core of an optical fiber. The principle of the FBG sensor is, when a broadband light spectrum passes through these fiber, the gratings reflects back a specific wavelength back towards the light source and allowing the rest to pass through without any interference. The shift in this wavelength that is reflected by the FBG is a response to change in mechanical strain and temperature for which it makes these sensors to be utilized for monitoring these conditions. A fiber optic cable can house multiple number of sensors. Each sensor reflects a specific wavelength and the shift in this reflected wavelength for all the fibers are measured and stored. To carryout this process, an external device called an interrogator is required. This device transmits the light and receives the reflection.

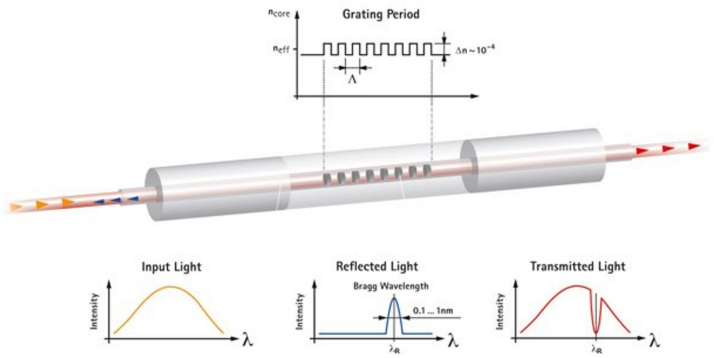

Figure 2.2: Structure and functionality of FBG sensor [1]

This specific reflected wavelength is called Bragg wavelength and can be defined as:

$$\lambda_B = 2\Lambda n_{\text{eff}} \tag{2.2}$$

Here, λ_B is the Bragg Wavelength, Λ is the periodic spacing of the grating element or grating's pitch, and n_{eff} is the effective refractive index of the optic core. External factors such as mechanical stress or temperature changes can alter both the pitch and effective refractive index, leading to changes in the Bragg wavelength.

FBGs are highly sensitive to temperature and strain. The mechanical strains influence the grating period and refractive index through photo-elastic effect whereas the change in temperature affects the FBG by thermal expansion and the thermo-optic effect. The sensitivity of the FBG can be measured using α and β by:

$$\Delta\lambda_B = \alpha\Delta\epsilon + \beta\Delta T \tag{2.3}$$

where, $\Delta\lambda_B$ is the change in Bragg wavelength, $\alpha\Delta\epsilon$ is the change in strain, and $\beta\Delta T$ is the change in temperature, and α and β are the FBG sensitivity factors to

strain and temperature.

Here is an figure for understanding of how the sensor reacts for strained and unstrained conditions.

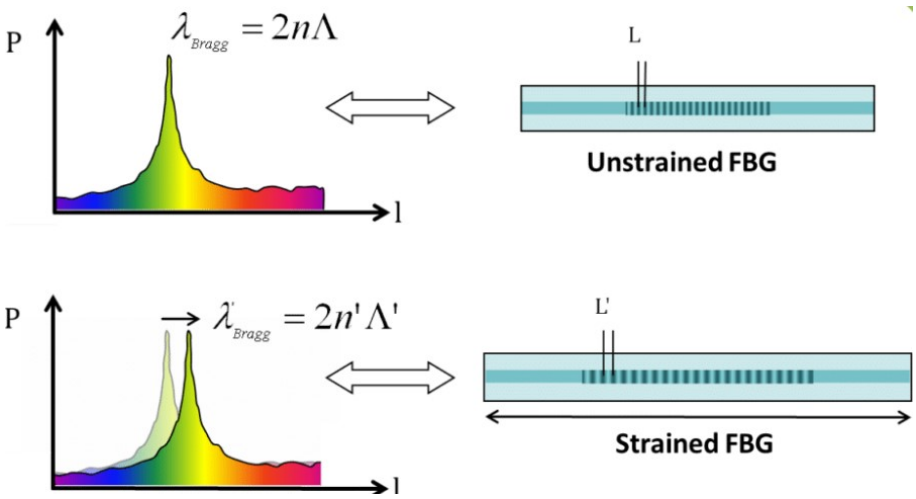

Figure 2.3: Illustration of the behavior of Fiber Bragg Gratings [2]

In the standard calibration provided by Sentea for the FBG sensors towards the mechanical strain and temperature variations, the calibration specifies that $1\mu\epsilon$ (microstrain) corresponds to wavelength shift of 1pm (picometer). And as for the temperature variations of $1°C$ results in wavelength shift of 10pm (picometers). These sensitivity calibration allows us to detect any minute changes within the sensors which is critical in applications for strain monitoring and provide us accurate measurements.

2.2.1 Applications of FBG

Fiber Bragg gratings have been widely used in aerospace engineering, civil engineering, structural health monitoring and medicine and health[11]. For instances, FBGs are embedded in composite materials to monitor the health of aircraft structures or used in civil engineering to assess the integrity of bridges.

2.2.2 Advantages of FBG

There are many advantage of using an FBG sensor instead of a conventional sensors.

- The most important advantage is that the sensor is immune to EMI.
- They are very small in size and can hence fit into complex spaces.
- FBG sensors are very flexible.
- Multiplexing can be done with a single fiber, this allows to measure multiple points of an object and multiple factors too.

2.3 FBG Interrogation

Interrogation is a process of measuring the reflected wavelength of an FBG sensor or series of sensors, and determine the change in strain, temperature, pressure,etc. Interrogation can either be done on only one sensor or can be done on multiple sensors. Interrogation of multiple sensors is called multiplexing. The are multiple methods of multiplexing and they are wavelength division multiplexing(WDM), time division multiplexing(TDM), and Spacial Division Multiplexing(SDM)[12].

In this thesis, the method used will be wavelength division multiplexing. We use a device called an Interrogator to carry out the process. Multiple fibers with multiple sensors can be connected to this device. The purpose of this device is to transmit the light signals, and capture the reflected wavelength and measure the shift in the wavelengths and store the data. The interrogator is calibrated to use the WDM method as there are multiple fibers with multiple sensors in use at a time. This is one of the advantages of WDM method of interrogation. For each sensor in a fiber, the reflected wavelength can be distinguished based on their bragg wavelengths. This difference in the bragg wavelength for each sensors in the same fiber can be done by varying the distance in the grating for each sensor which therefore, gives varying wavelength for each sensor. According to [12], generally the light sources for such setups emits light at 1550 nm and has a spectral range of 100 nm and each sensor in a fiber can have a dynamic wavelength range of 5 nm that way consisting upto 20 FBG sensors. This claim by [12] very close to right for our setup. The light source measurement is at 1510 nm and ranges upto 1560 nm as the sensors in the fibers we are using ranges from 8 to 10 and according to our observation the dynamic range for a sensor in the fiber is about 2 nm.

2.3.1 Advantages of WDM

- It is highly accurate compared to other type[12].
- It has more capacity, multiple signals can be transmitted from the same fiber at a time.
- It is flexible an can accommodate wide range of wavelength.
- It is cost effective as it ranges around 15-50 thousand euros for the system with sensors costs ranging from 80-200 euros. This is comparatively less from others[12].

2.4 Electric Machines

Whenever we talk about electric cars it's important to talk about the electric drive-train and in the electric drive train comes the electric machine which is most important. Electric machines are an important part in the drive-train as the purpose of it is to transform the electrical energy from the batteries to the mechanical energy the propels the vehicles. An electric machine can act as both electric motor and electric generator inside a car. The function of the motor is to propel the car by converting the electrical energy into mechanical whereas, the function of the electric generator

is to refuel the battery[13]. There are multiple requirements these machines need to satisfy before being used in the drive-train irrespective of their type. The machines needs to be highly efficient, have high starting and rated torque, wide speed range, etc[14].

One of the main reasons as to why the world is shifting towards the use of EM in vehicles is because of its power densities. It is comparable or at times exceeds internal combustion engine(ICE)[15]. Since the introduction of EVs with Electric Machines, there have been significant changes for the type of machines that is supposed to be used in EVs. This is due to fact that different machines satisfy different requirements and some EVs equip multiple machines to satisfy the requirements. There is also the factor of cost, the pricing should be acceptable[14]. The most basic types of Electric Machines used in EVs/HEVs are the induction machines, PMSM, etc, and there are various types that have the potential to be used.[15][14]. The following picture gives us an understanding of the types of machines that can be used in the vehicles as of now.

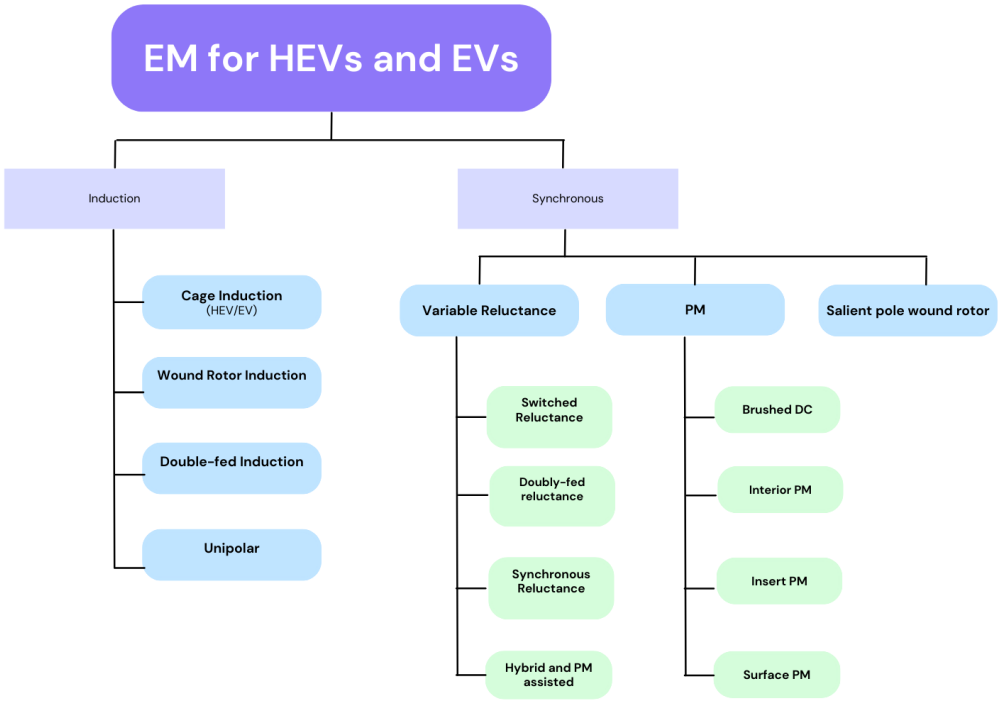

Figure 2.4: EM for HEVs and EVs(adapted from [3])

We will be using one such electric machine and carry out various tests on it. The type of machine used is PMSM(permanent magnet synchronous machine) with a rated torque of 490 Nm. The rotor magnets of the PMSM are embedded inside the rotor of the machine creating a small and uniform airgap between rotor and the stator. The power output of the PMSM used is about 220-240 kW with a maximum speed of 14,000 RPM. The power output is software dependent. It basically means the power output is controlled by software control algorithm that governs

their behaviour. By this method, performance, efficiency, and the reliability of the propulsion system can be optimized.

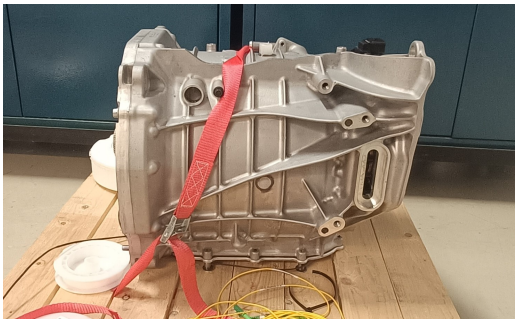

(a) Side view of EM

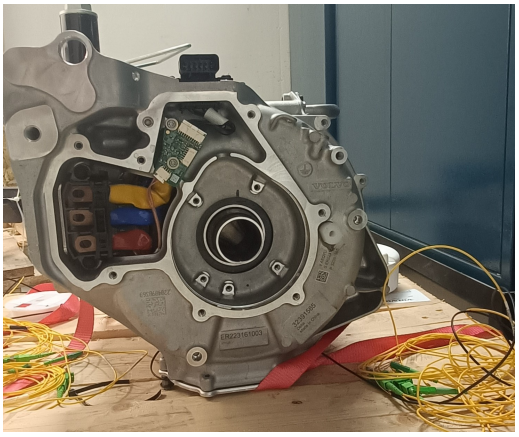

(b) Front view of EM

Figure 2.5: MEP2 ERAD

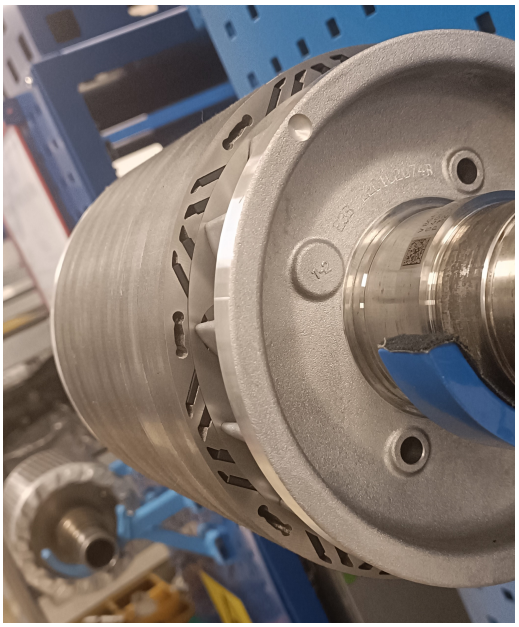

(a) Rotor used in ERAD

(b) magnet positioning

Figure 2.6: Rotor and magnet location

This electrical machines are a combination of both mechanical components and electrical components. The parts are as follows:

1. **Mechanical**:The mechanical parts of the EM are the rotor, the rotor shaft, bearings on the either sides of the EM, and cooling systems such as cooling channels for liquid cooling and the fans.
2. **Electrical**:Electrical parts are the Stator, stator winding, magnets on the rotor, the inverter, and various sensors.

2.5 Bearings

Bearings are components that has the ability to reduce friction and wear between two relative parts.They also offer support and are very useful in transferring loads. These components are very much essential in machines. It basically is called as the machinery joint[16]. Based on the different requirements of a machinery, there are various types of bearings that can used.
The bearings are classified based on their rolling elements such as ball bearings, roller bearings, plane and magnetic bearings. The following are the different types of bearings:

- Deep groove ball bearings.
- Self Aligning ball bearings.
- Thrust ball bearings.
- Angular contact ball bearings.
- Tapered roller bearings.
- Spherical roller bearings.
- Cylindrical roller bearings.
- Needle roller bearings.
- Magnetic Bearing.
- Plain Bearing.
- Fluid bearing.
- Linear bearing.

The machine used is equipped with the deep groove ball bearings. The reason for selecting this particular bearing type is because it can bear both radial as well as axial load condition[16].

Figure 2.7: Different types of bearings[4]

2.5.1 Deep Groove Ball Bearings

The bearings being used for this thesis is a deep groove ball bearings. They are the widely used bearings and are available in different configuration that is single row and double row. By the straight forward design of the single row configuration, it is most commonly adapted[17]. These bearings are designed to handle high speed operations with very minimal maintenance and allows them to support axial loads any direction possible.

A general ball bearing consist of seal, cage, ball/rollers, inner ring and outer ring which is represented in the fig:

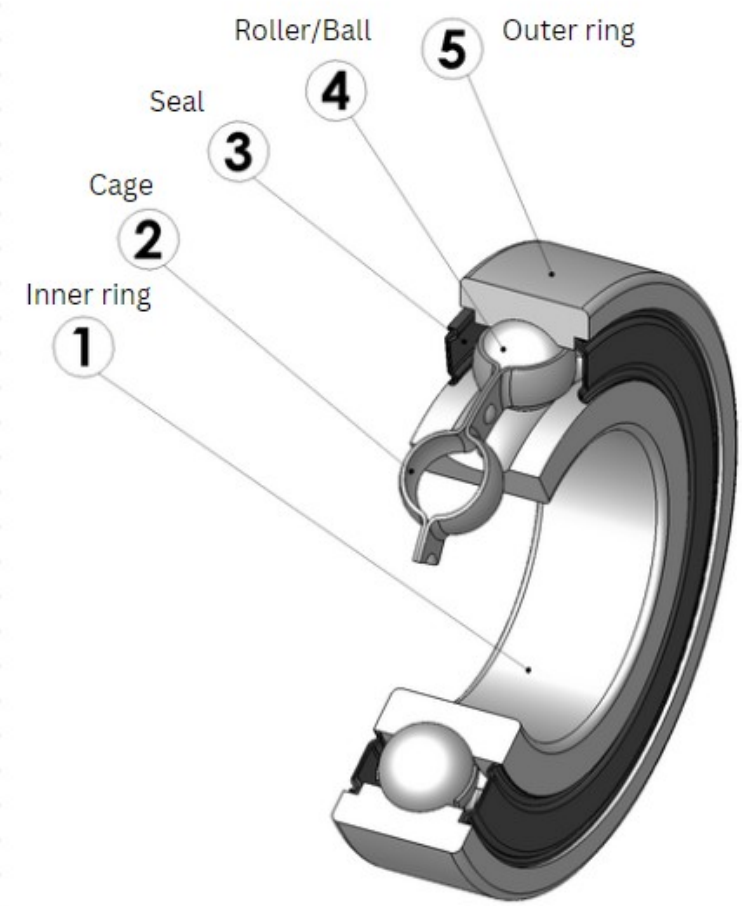

Figure 2.8: Schematic structure of ball bearing

- **Outer Ring**: It is also known as the outer race, which is particularly designed to withstand external loads and harsh environments. It is thicker and made from hardened steel for enhanced durability[18].

- **Inner Ring**: The inner ring or inner race, directly interfaces with the shaft and is necessary for the accurate transmission of forces. They ensure precision fit to avoid any misalignment that can affect its performance and longevity[18].

- **Cage**: The cage maintains a uniform distribution of the balls, preventing any contact between them and provides consistent performance[18].

- **Ball**: The bearings have spherical balls keep the contact area as minimal as possible, which reduces friction and allows bearing to operate smoothly at very high speeds. The rings and balls of the bearings are of high-carbon chromium bearing steel which provides excellent durability and resistance to wear and tear[18].

- **Seals**: These are very essential for preventing contamination of the bearing from foreign particles and also keeps the lubricant inside the bearing. The seals

offer maximum protection without significantly increasing the heat or torque. The bearings can be equipped with seals and are often pre-lubricated with a grease which is lithium based, suitable for specific operational needs[18].

2.5.2 Observable changes in rotor bearings

In an electrical machines, bearings play a very important role as they are subjected to constant loading and unloading. The primary load contributors for it are from the transmission part of the machines and electrical part of the machines.

From transmission(Gear mesh forces)

- **Radial load from planet load sharing**: In an electric machines that incorporate planetary gear systems, radial loads arise due to interaction between the sun gear, ring gear and planet gear. From the figure 2.9, we see there are three planet gear around the sun gear. When torque is applied to the sun gear, it drives the planet gears, which mesh with the ring gear and distribute the torque evenly and this interaction generates radial forces within the gears.

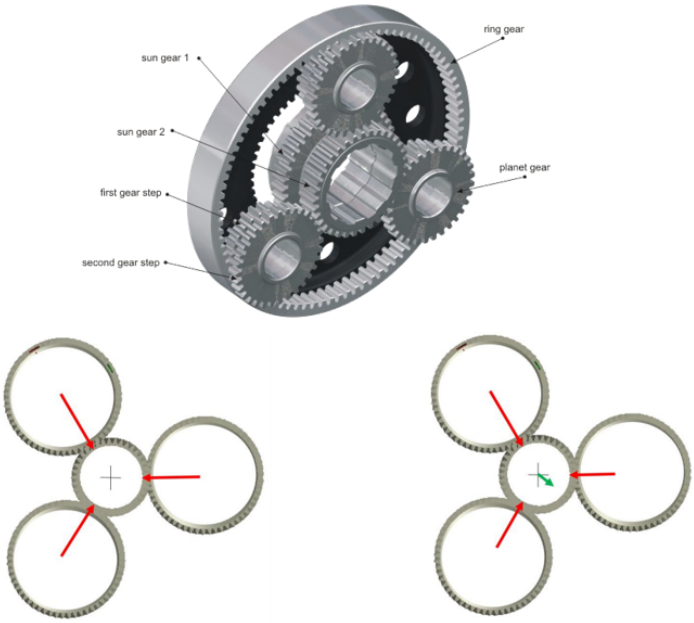

Figure 2.9: Radial force due to Planetary Load Sharing [5]

- **Axial load from the sun gear**: Axial forces in the gear systems are primarily generated by the sun gear. These forces arise due to helix angled gear system which creates component of force that pushes the sun gear along the drive shaft, which leads to axial loads on the bearings and misalignment issues.

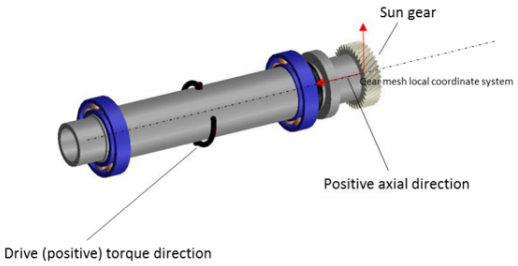

Figure 2.10: Axial force due to sun-gear

From electric machine

- Unbalanced magnetic pull: This can occur if the stator and rotor are not in an alignment. The rotor being the rotating part here may experience some radial pull due to this or at times even when the magnetic field around the stator is uneven due to the rotor being closer to the stator in one position. This can cause lot of vibration which can induce a lot of stress on the bearing and therefore wear and tear of the bearing.

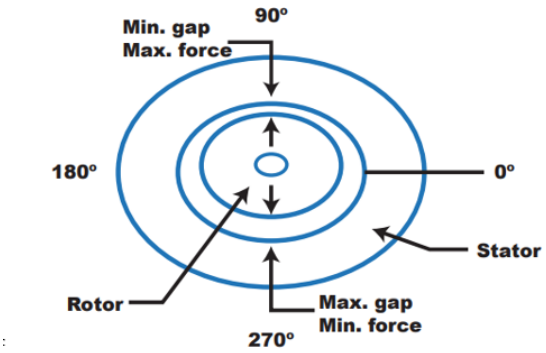

Figure 2.11: Unbalanced Magnetic Pull

- Axial skewing force: When an object rotating, in this case the rotor is tilting towards a particular direction rather than rotating along its axis, it is called a Axial skewing force. There are reasons why such a thing can happen such as misalignment of rotor during the assembly of the motor, uneven air gap between the rotor and the stator and even wear and tear. The figure above can represents the skewing force due to uneven air gap.

Apart from the these forces, the bearing can also experience temperature changes and the sensor is sensitive enough to measure the local temperature changes and with multiple sensors along different points of the bearings, it temperature gradient and therefore can give an idea of the heat distribution in the bearings. The vibrations occurring in the bearing can also be measured by the sensors and this can basically help out in fault detection. By focusing on a single sensors, it is also possible to measure the no.of balls passing per second.

3
Methodology

In this section we discuss on the methods undertaken over the duration of this thesis project to investigate the application of Fiber Bragg Grating sensors for monitoring the axial strain of the mechanical ball bearings of an electric motor.

To achieve the main goal of this thesis, planning was done by dividing the scope into sub-tasks which are:

1. Preliminary Research
2. Python-based interrogator software
3. Test setup development
4. Graphic User Interface (GUI) to capture data
5. Data analysis and post process

3.1 Preliminary Research

A preliminary stage is conducted involving investigation and exploration of relevant research papers, previous reports and comprehensive review of documents to ensure a thorough understanding of the subject and its current technology. The review mainly focuses on the application and advancements in FBG sensor technology, the operation and capabilities of optical interrogators, and mechanical characteristics and operational stresses of the ball bearings. The aim in this task is to gather all important and essential concepts and findings from previous works to establish a solid theoretical foundation of the thesis project. This foundational knowledge will help guide in the development in the next steps going forward.

3.2 Python-based Interrogator software

The second phase of the project was to have a python function that facilitate the axial strain acting on the sensor wrapped FBG sensors. This step was pivotal for capturing and managing the sensor data from the interrogator.

3.2.1 Software Interface

The functionality of the Sentea interrogator can be visualized using the the available software interface, where one is the Sentea PeakViewer or using an Application Programming Interface (API) for python from Sentea.

3.2.1.1 PeakViewer

The Peak Viewer from Sentea is an internal software that is designed to enhance the analysis of spectral data captured by the interrogator. This software provides robust method for visualizing, processing and analyzing the reflection spectra, making it an essential resource for the study on FBG sensors and its measurement system.

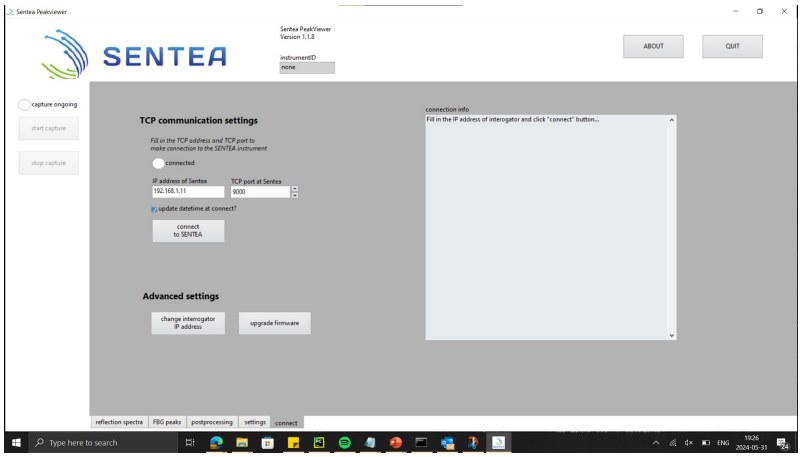

Figure 3.1: SENTEA PeakViewer Software Application

The functionality of Sentea Peak Viewer is distinguished by its advanced graphical capabilities for visualizing the reflection spectra data for analysis. This visualization is instrumental in rapidly identifying and analyzing characteristic peaks and anomalies, crucial for monitoring physical phenomena. At the core of its functionality, the software's sophisticated peak detection module employs advanced algorithms that users can adjust in terms of sensitivity and threshold, enabling precise customization to fit various experimental conditions and sensor configurations. Moreover, the Peak Viewer enhances spectral analysis accuracy through robust data filtering and processing tools that effectively reduce noise and remove extraneous data points, clarifying spectral signals and improving the reliability of peak detection and analysis, particularly in environments with substantial background noise.

3.2.1.2 API

The sentea.interrogator API is python coded program that provides comprehensive set of tools for interacting with the interrogator. It provides functionality to access and configure a Sentea interrogator device and is designed to be as stateless as possible, to allow seamless concurrent access via other interfaces for example this thesis project in terms of GUI and API driven scripts.[6]

- **Overview of Sentea Interrogator API**: The API offers comprehensive tools for interaction with the Sentea Interrogator DM-8120, designed to be stateless to facilitate seamless concurrent access.
- **Connection Management**:

  - Managed via a `Client` object, either instantiated directly or through a context manager.
  - Recommended use of a context manager to handle automatic connection closures.
- **Configuration of Peak Detection**:
  - Detailed configuration via the `peak_detection` attribute.
  - Allows setting of detection methods and thresholds for precision based on operational needs.
- **Data Capture Functionality**:
  - Accessed via the `capture` attribute.
  - Configurable settings for capture modes, sample rates, and content types.
  - Functions to start and stop data capture, with options to select specific fibers.
- **System Functions**:
  - Provides access to system-level settings and properties.
  - Includes setting system time and retrieving system identifiers and fiber count.

3.2.2 GUI for capturing the FBG sensor data

One of the main task of this thesis project was to develop a graphic-user interface (GUI) to capture the sample data/sensor data and save them in the required file directory. The main reason of the GUI is for simplifying the capture process in future and this would be essential for tests with higher sample frequency and speed, which is highly recommended by Sentea to use the API for this above requirements.

- **Concept**
  The concept development for the GUI for the interrogator was aimed to simplify the complex fiber optics sensor operations, which consists of several features from the sentea interrogator API and visualization idea from the PeakViewer. The GUI is designed to be intuitive, allowing users to manage connections, configure data capture settings which is the sample frequency and threshold, visualize the peaks and save the results in real time without the need of any extensive technical knowledge. Through user-centric approach, each functional interface was made to ensure seamless operation.This conceptualization was crucial in transforming sophisticated monitoring technology into a practical tool accessible to both novice and experienced users.

- **Visualization**

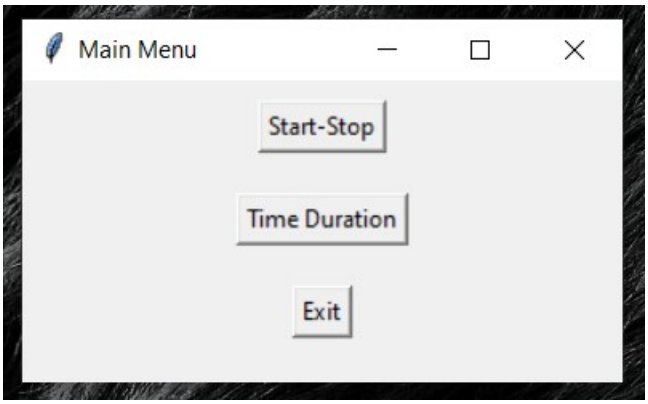

Figure 3.2: Main Menu of the GUI

For the convenience of our project two GUIs were created, one with time duration figure refer and another with start-stop functionality. It was decided to capture the sample data for particular period of time for analysing purpose, so the GUI with time duration function was made to collect sample data for user-defined time period whereas, the GUI with start-stop function can capture the data for 'n' seconds of time depending on the test requirements.

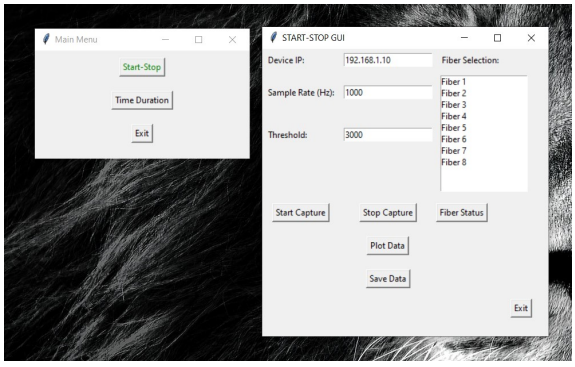

(a) Start-Stop GUI

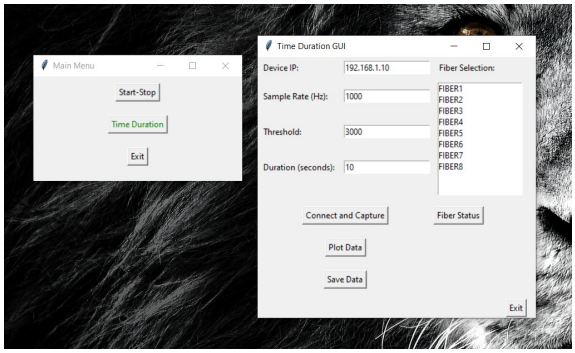

(b) Time Duration GUI

Figure 3.3: Visualization of GUI

- **Functionalities**
  - Connection Management: The first step in GUI is to establish a connection with the interrogator. It is straight forward method for inputting the IP address and managing the connection.

  - Data Capture Configuration: The capture settings of the sensor data can be set by the users. They can set the sample rate/frequency, threshold value and select the fiber channel for which fiber data to be captured.

  - Real time data visualization: Once all the above requirements are set, this functionality is built on the ability to retrieve and handle data streams from multiple fibers simultaneously. It can also plot the fiber peaks with respect to the timestamp.

  - Data export and management: The GUI allows to save and manage the sample data by exporting the data in the CSV format. This ensures that users can easily archive, share, and further analyze the data outside of the GUI environment.

3.3 Test setup development for applying axial strain on bearing

In order to verify whether this FBG technology can be used to measure or track the change in strain, we needed to design and develop a test setup. This was one of the sub-tasks of our thesis. To accomplish this task, we divided the task into multiple steps.

1. Firstly, a concept was planned and discussed on how we will be applying the load onto the bearings.
2. We designed and developed components that were necessary to carry out the tests.
3. Setting up a test environment for us to carry out the test. The necessary tools, devices required were made available for the tests or at least till the duration of the tests.
4. Once the components and test environment were ready, we need to make sure that they are working the way they should and we expect them to be, else re-design and manufacture the components.
5. The tests was carried out for different loading points.
6. Post processing was further carried out.

3.3.1 Concept planning

The first part of the testing was to develop a test set-up where we can apply an axial load to the rotor shaft of an electric machine and the manage the rotation of the shaft. It was discussed and decided that we use an hydraulic press machine for this. This method was thought out only for axial load purpose and not anything else. With the help of Volvo, we were able to acquire a hydraulic press machine for the duration of our thesis.

In order to give apply the load, it was decided to invert the entire electric machine upright and place it on the hydraulic press machine. Then with the help of a battery powered hand drill, the machine was rotated. A point to be noted is that the non-driving end was facing the press piston. It was also decided to monitor the axial force being applied onto the machines. We used an additional force sensor to monitor it.

3.3.2 Design and Manufacturing

To apply a load from the press, the object or component in contact must be stable. When rotation is given, we can't apply load directly onto the shaft as the friction can cause lot of heat, and it can also damage the shaft. Therefore, with the help of a colleague, two plates were designed and manufactured that sits on top of the non-driving end in between which there's a rotating element(wheel hub) that prevents the top plate from rotating during a test. The bottom plate sits on the shaft, then the wheel hub that restricts the rotation onto the top plate, and on top of the wheel hub is a top plate onto which we apply the load from the press.

Figure 3.4: Top plate

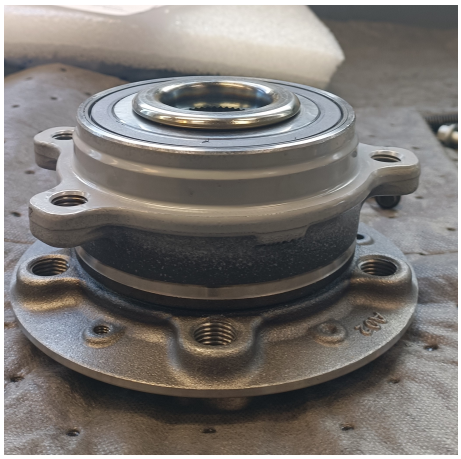

Figure 3.5: Wheel Hub

The initial design for the bottom plate had some issues. The diameter of the shaft was 46.2 mm, and the diameter of the center steering of the lower plate was 49 mm. There was a significant play at the center steering, which caused the lower plate to wobble a lot during rotation, presenting a problem. With a total tolerance play of nearly 4 mm and a depth of just 3 mm, there were chances for the bottom plate to slip off from the shaft.

(a)

(b)

Figure 3.6: Initial design of Bottom plate

It was then suggested to redesign the bottom plate to have a conical shape with more depth about 8.14 mm and decrease the diameter by 2mm thereby having a tolerance of 1 mm, in the center steering. The new dimensions are 47.1 mm diameter for the

center steering and the depth is 8.14 mm. This change would allow the rotor shaft to fit more securely inside the center steering and minimize wobbling. Additionally, three holes were drilled into the bottom plate to fix it to the wheel hub using nuts.

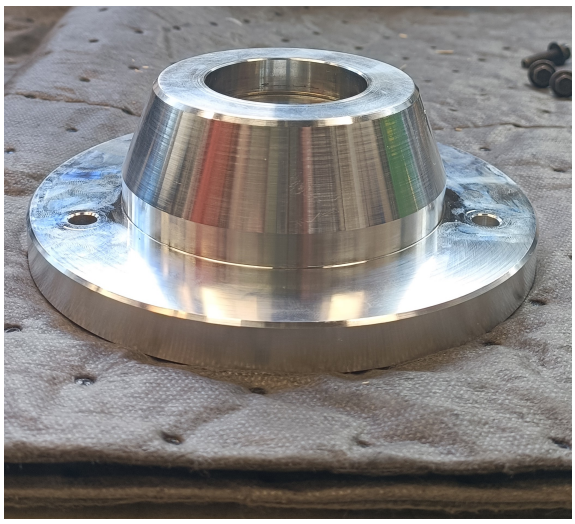

Figure 3.7: New design of the bottom plate

The top plate design was made such that it could accommodate the force transducer on top of it. Holes were drilled onto it to fix the transducer to it and also to fix the plate to the wheel hub. With everything setup and fixed together we could rotate the motor without in-turn rotating the force transducer for even distribution of the axial load applied from the hydraulic machine.

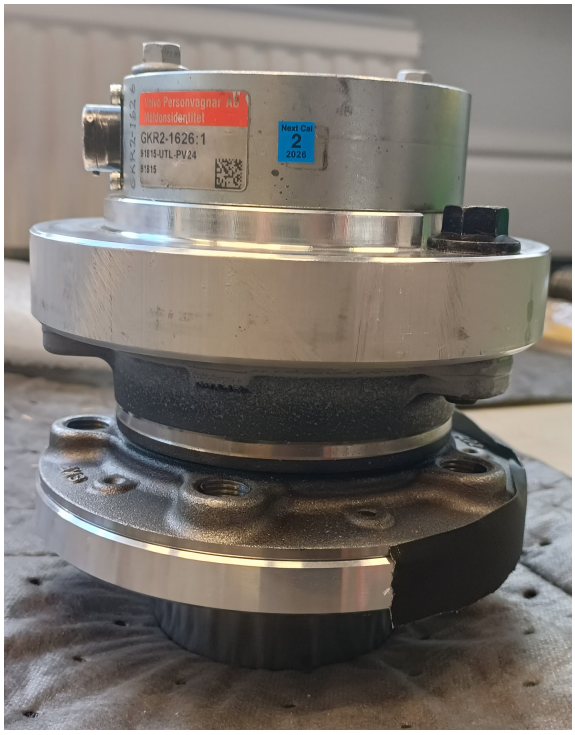

Figure 3.8: Final Design Setup

3.3.3 Test Environment setup

While the components were being manufactured, the test environment was being setup. In order to carry out this test, the following were required:

- **Hydraulic press**: As discussed in Subsection 3.3.1, the hydraulic press machine was acquired for the duration of the thesis. The maximum limit of the press machine was about 20 tons. The machine used was a mechanically operated hydraulic press. It had two levers to it, the left lever was used for higher increments of load and the right lever was used for lower increments. There's also a knob rotating which will release the load. A force transducer was connected to the press to measure the amount of force being applied. We did not make use of it since we did not know weather it was calibrated.

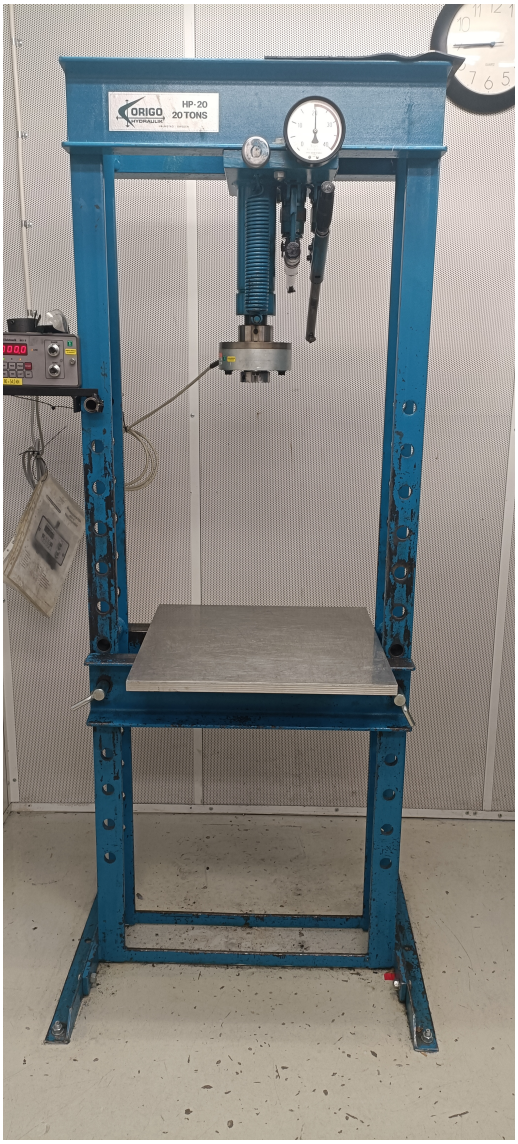

Figure 3.9: Hydraulic Press

- **Electric Machine**: The electric machine we used was an MEP2 ERAD. The inverter of the machine is removed and the FBG fibers are connected to the either side of the rotor shaft from the bottom of the machine. The machine is in inverted position during testing and placed carefully such that the axis of the shaft and the axis of the hydraulic press are aligned. This ensures that the load applied onto the bearing is distributed equally.

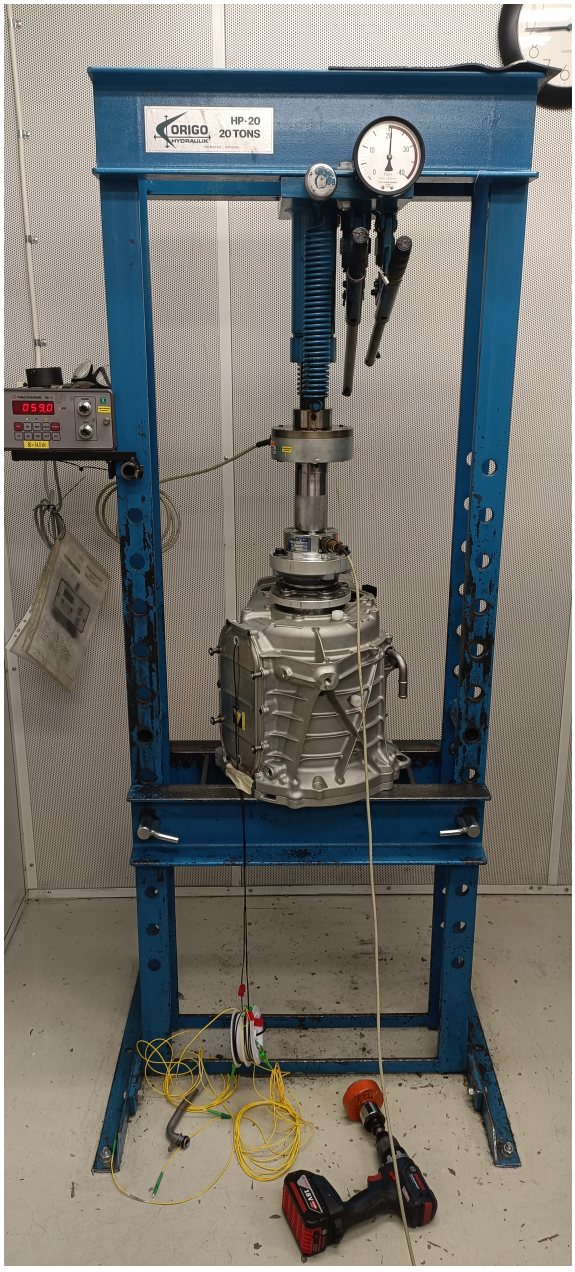

Figure 3.10: Hydraulic Press with electric machine

- **The Sentea Interrogator**: To capture the sensor data by the dynamic changes in the mechanical stress experienced by the ball bearings, the Sentea interrogator DM-8120 is used. It is a high performance optical sensor

interrogator designed for precise and rapid monitoring of the FBG sensors.

Figure 3.11: Sentea Interrogator

Specification	**Value**
Wavelength Range	1525 nm to 1575 nm
Wavelength Resolution	1 pm
Wavelength Accuracy	10 pm
Wavelength Sensitivity	0.1 pm
Number of Channels	8
Max. Sample Frequency	24KHz
Measurement Accuracy	±2 pm
Interface	Ethernet

Table 3.1: Technical Specifications of the Sentea Interrogator DM-8120 [6]

- **Force transducer**: To monitor the force/load being applied, a force transducer of capacity 20 KN is used.

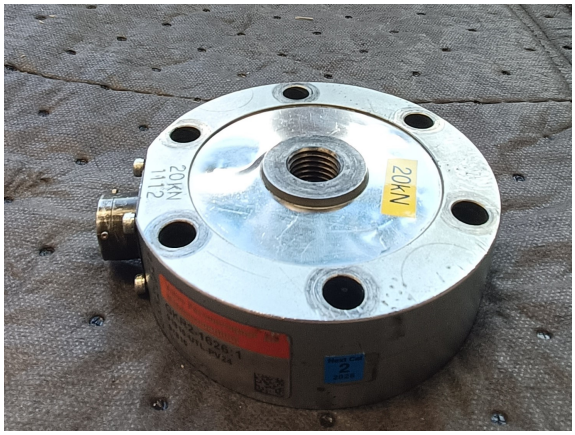

Figure 3.12: Force Transducer

- **Dewesoft for force measurement**: It is amplifier we have used to measure the force from the force sensors placed on the top plate. The force sensor is connected to it. The amplifier is then connected to the system with a usb type connector. In order to access the outputs of the amplifier, we make use of a software called DewesoftX(64-bit). The calibration of this device was done by one of our colleagues here at Volvo cars.

Figure 3.13: Dewesoft Amplifier and software

- **Hand-drill and mount**: The tests were conducted with the help of a hand drill. In order to rotate the shaft, we made use of a hand drill that had two different modes. Mode 1 is 600 rpm and mode 2 is about 1900 rpm.To run the machine with the hand drill, a mount as shown below was used to mesh with the shaft teeth.

(a) Mount front view

(b) mount side view

Figure 3.14: Hand drill mount

- **Tachometer**: To get an idea about how fast the shaft was rotating considering the weight of the force transducer, rotor, plates along with wheel-hub, and the added axial force, we used a tachometer.

Figure 3.15: Tachometer

3.3.4 FBG sensor installation

The machine consists of 4 FBG fibers installed on it. The fiber installation was already done by a company name "Sensing 360". Two fibers were attached to the Driving end(DE) bearing of the rotor, and the other two to the Non-Driving end(NDE) bearing of the rotor. The fiber are not directly attached to the bearings, Sensing 360 have used a smart photonic sleeve to which the fibers were wrapped and parallel to each other. This sleeve was then pressfit to the bearing. The pressfit to the bearing gives a compressive strain of -3.5E-4 in fiber 1 and -3.8E-4 in fiber 2. A tensile strain is added on the application of axial force.

As mentioned above, each bearing has two fibers wrapped around its circumference. One of the fiber in both bearings has 1 sensor extra compared to the other fiber i.e., fiber 1 has 9 gratings(sensors) and fiber 2 has 8 gratings. The extra sensors on both the fiber was for temperature measurement purpose alone.

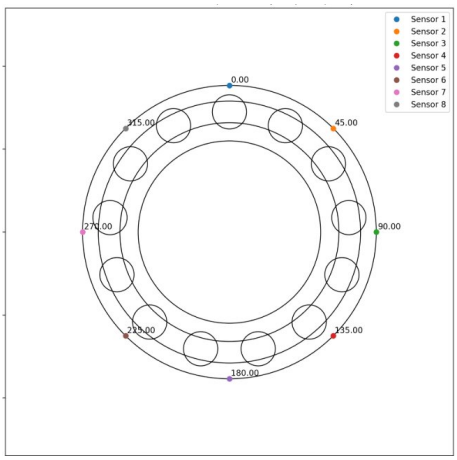

(a) Sensor position around the bearing

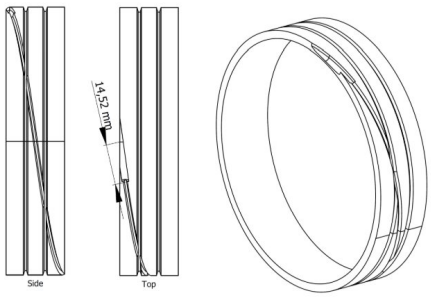

(b) Fiber position on bearing

Figure 3.16: FBG fiber and sleeve

3.3.5 Experiment

The experiment was carried out in only one mode of the hand drill i.e., at 600rpm. It was decided as it will be hard the maintain the stability above 1000 rpm and it would result in too many noises. However, the test were for different loading conditions and for both driving end(DE) and non-driving end(NDE) seperately.
During the test, there were some key points we needed to focus on. One of the most important factor was the weight of the rotor acting on the rotor bearing of the DE, and the additional weight from the transducer, wheel-hub, the plates, and the bearing from the NDE. The combined weight of the transducer, plates and wheel-hub is 7.26 kgs and the rotor weight is approximately 30kgs. So that is total of 365.45 Newtons on top of the loads we were testing at. The loads at which the tests were carried out are:

Table 3.2: Loading conditions

Loads (N)	Existing load(N)	Total load(N)
500	365.45	865.45
1000	365.45	1365.45
1500	365.45	1865.45
2000	365.45	2365.45
2500	365.45	2865.45
3000	365.45	3365.45
4000	365.45	4365.45
5000	365.45	5365.45

The second important factor we needed to consider was that there was no radial force acting on the FBG sensor. As the fibers are wrapped around the bearing and the machine itself is in inverted position.

To begin with the tests, first we connected the fibers to the interrogator. The interrogator was then connected to our laptop using an Ethernet cable. Once the connection was established, we connected the force transducer to the dewesoft amplifier and that to our system using as USB cable. Once we connected the amplifier, we had to set the reading to zero as there was no load on the transducer yet. We verified if the transducer is working by applying some load onto it. After all the devices were connected and checked, we started running the tests for the above mentioned loads at 600 rpm. During each tests, we checked the rpm by directing the tachometer to the bottom plate. The tests for each load was done for 10 seconds. The sampling rate was set to 1000 Hz and the threshold was set to 3000. To carry out this tests and to set the above settings, the GUI we developed was used. Once the tests were done, it was saved in the csv format.

3.4 Post processing

Tests were conducted for DE and NDE separately. The data we get using the interrogator is alternate i.e., interrogator samples the fiber 1 and 2 simultaneously but one after the other. The data we get is in the following form.

	timestamp	fiber_id	peak1	peak2	peak3	peak4	peak5	peak6	peak7	peak8	peak9	peak10
0	2024-05-14 14:15:13.999911	2	1512.500834	1517.733377	1528.884551	1534.091717	1538.935215	1544.307756	1549.631321	1554.883619	NaN	NaN
1	2024-05-14 14:15:13.999911	1	1512.611947	1517.485536	1528.952700	1533.824473	1534.673545	1539.571632	1544.540496	1549.537392	1555.070213	1560.190403
2	2024-05-14 14:15:13.999911	2	1512.499807	1517.731941	1528.879649	1534.091761	1538.935194	1544.349726	1549.631309	1554.878938	NaN	NaN
3	2024-05-14 14:15:13.999911	1	1512.610585	1517.487431	1528.952692	1533.824305	1534.673645	1539.571594	1544.540684	1549.537246	1555.069626	1560.217747
4	2024-05-14 14:15:13.999911	2	1512.500395	1517.733151	1528.879982	1534.091796	1538.935184	1544.405775	1549.631310	1554.876097	NaN	NaN
...	...	...	...	...	...	...	...	...	...	...	...	...
8039	2024-05-14 14:15:23.990964	1	1512.612250	1517.489005	1528.952684	1533.824440	1534.673572	1539.571628	1544.540867	1549.537324	1555.078410	1560.227972
8040	2024-05-14 14:15:23.990964	2	1512.504159	1517.735065	1528.891764	1534.091897	1538.935183	1544.449948	1549.631293	1554.881218	NaN	NaN
8041	2024-05-14 14:15:23.990964	1	1512.612880	1517.492180	1528.952692	1533.824444	1534.673751	1539.571580	1544.540992	1549.537170	1555.075039	1560.252251
8042	2024-05-14 14:15:23.990964	2	1512.505284	1517.738306	1528.901649	1534.091912	1538.935183	1544.512212	1549.631288	1554.879775	NaN	NaN
8043	2024-05-14 14:15:23.990964	1	1512.614552	1517.493366	1528.952701	1533.824412	1534.673359	1539.571592	1544.541474	1549.537058	1555.073328	1560.218255

Figure 3.17: Sample data

Initially, we checked the data for any errors, NaNs, emplty cells, etc. Once such rows or columns were dropped, we separated the data based on their fiber ids. After separating the data, all the peaks vs the time(seconds) was plotted to check if we are getting the trend as expected. In order to check for the strain, we had to find the delta value for each sample for which we needed to select a reference value. After couple of discussion with our supervisors, it was decided to take the average value of each peak as the reference for that peak and subtract it with its respective peaks. This will give us the delta value in nanometer(nm). We know that from 2.2 in Chapter2, 1 picometer(pm) is equal to 1 microstrain, we should convert the delta wavelength shift into picometer. This gives us the microstrain from the FBG sensors.

$$\delta\lambda_B = \lambda_B - \lambda_{\text{ref}} \tag{3.1}$$

$$\epsilon = \lambda_B \times 1000 \tag{3.2}$$

Further a function was created to randomly pick a section of data and plot it against the time. The length of that data was about 1000 samples out of the total sample. This was done for the entire dataframe i.e., for all the peaks. This data was further filtered using the butter worth filter function. It is to be noted that, despite setting the sample rate of 1000 Hz altogether, each fiber was sampled at 400 Hz each and the total was 800 Hz. To calculate sampling rate

$$\text{Sample rate} = \frac{\text{no. of samples per fiber}}{\text{sampling duration}} \tag{3.3}$$

Therefore, the sample rate of 400 is used according to the data we've to filter the data. Plots of original data vs filtered data for all the peaks of all fiber at different loads have been plotted. The discrete Fourier transform for the data is done in order to check how many times the ball passes a particular sensor. With the help of BPFO, it was also possible to calculate the RPM of the shaft. To validate if the BPFO is giving the correct RPS, it was necessary to use the simulation BPF which is based on one rotation of the shaft. This value was used in a simple formula that gives a RPM of the shaft. A function was crearted to calculate the same. This value was verified with the RPM from tachometer.

The relationship between the shaft RPS, BPF, and observed frequency(BPFO) is as follows:

$$\text{BPFO} = \text{BPF} \times \text{RPS of shaft} \tag{3.4}$$

The sensor data that was converted into strain data using the calibration factor and using some basic formula, stress sustained by the material was calculated.

$$\text{Youngs' Modulus} = \frac{\sigma}{\epsilon} \tag{3.5}$$

$$\text{Force} = \sigma * \text{cross section area} \tag{3.6}$$

We know there are 2 fibers wrapped around the bearing parallel to each other. This means each sensor in fiber1 is parallel to the corresponding sensor in fiber 2. From the strain equation using the calibration factor above, we can find strain for sensors in both the fibers. Assuming there is uniform strain distribution, we'll take the average of the strain values from both the fiber. For the average strain value, we can find the stress using the young's modulus of the bearing.

$$\epsilon_(avg) = \frac{\epsilon_1 + \epsilon_2}{2} \tag{3.7}$$

And for the area, we assumed since the fiber are stuck to the outer ring surface, the cross-sectional area of the outer ring would be sufficient.

$$\text{cross section area} = 2 \times \pi \times r_o \times \text{width} \tag{3.8}$$

where r_o is the outer radius of the bearing, and width is the thickness of the outer ring.

4

Results

4.1 GUI

In this section we are going to see the visualization of each functionalities of the Graphic User Interface of the interrogator.

- **GUI selection** First, you get two options to select the type of GUI based on the test requirements, which is either the start-stop GUI or time-duration GUI.
  Insert figure of GUI selection.
- **Sample Capturing**: After choosing the required GUI and entering all the functional requirements that is the connection IP address, sample frequency rate, threshold value and fiber selection. These are the common configuration settings for sample capture for both the GUIs. The sensor samples are obtained this way:
  - **For start-stop GUI**: After the configuration settings mentioned above is set, the start capture can be clicked which pops up a message that the capture is started (figure reference) and can be run for 'n' number of seconds based on the test period. After certain amount of time if the stop is pressed, the capturing process stops (insert refernece). Once stopped, a new window opens showing the sample data with respect to timestamp (inert reference).
  - **For time-duration GUI**: Similarly, set the required configuration settings and in this GUI you can mention the particular time duration for the samples to be captured which can be advantageous in many test methods. Once you press Connect and capture, you will have to wait for the amount of time set and once done you will get a message box indicating the capture is done and a new window with sample data appears which can be further used for analysis.

Sample Data

timestamp	fiber_id	peak1	peak2	peak3
2024-06-11 14:10:55.841779	1	1529.978565	1540.002027	1549.896679
2024-06-11 14:10:55.841779	1	1529.980424	1540.006842	1549.891078
2024-06-11 14:10:55.841779	1	1529.977669	1540.002767	1549.895151
2024-06-11 14:10:55.841779	1	1529.976221	1540.005254	1549.893672
2024-06-11 14:10:55.841779	1	1529.980693	1540.004899	1549.893968
2024-06-11 14:10:55.841779	1	1529.980468	1540.006748	1549.890163
2024-06-11 14:10:55.841779	1	1529.980865	1540.001312	1549.894946
2024-06-11 14:10:55.841779	1	1529.983134	1540.003564	1549.892153
2024-06-11 14:10:55.841779	1	1529.977268	1540.002696	1549.897269
2024-06-11 14:10:55.841779	1	1529.976150	1540.004616	1549.893933
2024-06-11 14:10:55.841779	1	1529.981143	1540.004161	1549.892993
2024-06-11 14:10:55.841779	1	1529.980977	1540.002095	1549.890538
2024-06-11 14:10:55.841779	1	1529.981151	1540.004249	1549.893399
2024-06-11 14:10:55.841779	1	1529.975094	1540.006907	1549.893284
2024-06-11 14:10:55.841779	1	1529.978176	1540.003212	1549.896571
2024-06-11 14:10:55.841779	1	1529.977183	1540.002748	1549.899446
2024-06-11 14:10:55.841779	1	1529.979163	1540.004238	1549.897257
2024-06-11 14:10:55.841779	1	1529.977934	1540.003521	1549.894224
2024-06-11 14:10:55.841779	1	1529.978100	1540.004235	1549.899025
2024-06-11 14:10:55.841779	1	1529.980582	1540.002458	1549.892322
2024-06-11 14:10:55.841779	1	1529.977441	1540.001735	1549.893580
2024-06-11 14:10:55.841779	1	1529.980993	1540.002625	1549.898029
2024-06-11 14:10:55.841779	1	1529.979449	1540.003545	1549.895149
2024-06-11 14:10:55.841779	1	1529.976049	1540.001802	1549.892236
2024-06-11 14:10:55.841779	1	1529.978936	1540.004869	1549.896774
2024-06-11 14:10:55.841779	1	1529.979334	1540.002211	1549.894763
2024-06-11 14:10:55.841779	1	1529.978599	1540.005751	1549.895037
2024-06-11 14:10:55.841779	1	1529.980359	1540.004742	1549.894160
2024-06-11 14:10:55.841779	1	1529.979521	1540.004205	1549.893624
2024-06-11 14:10:55.841779	1	1529.976897	1540.001831	1549.896694
2024-06-11 14:10:55.841779	1	1529.976566	1540.003326	1549.898055
2024-06-11 14:10:55.841779	1	1529.978811	1540.001460	1549.892738
2024-06-11 14:10:55.841779	1	1529.978612	1540.001326	1549.895331
2024-06-11 14:10:55.841779	1	1529.978790	1540.004092	1549.900186
2024-06-11 14:10:55.841779	1	1529.977004	1540.001345	1549.894980
2024-06-11 14:10:55.841779	1	1529.977520	1540.003874	1549.896147
2024-06-11 14:10:55.841779	1	1529.978632	1540.001577	1549.897000

Figure 4.1: Samples obtained from GUI

- **Plot Data**: After the sample data is captured successfully, the GUI has a function 'plot data', when clicked, the plot of the sensor peaks in the fiber with respect to timestamp is plotted and shown. Only the fiber selected before capturing gets plotted and these plots can be used to visualize and verify the sample data.

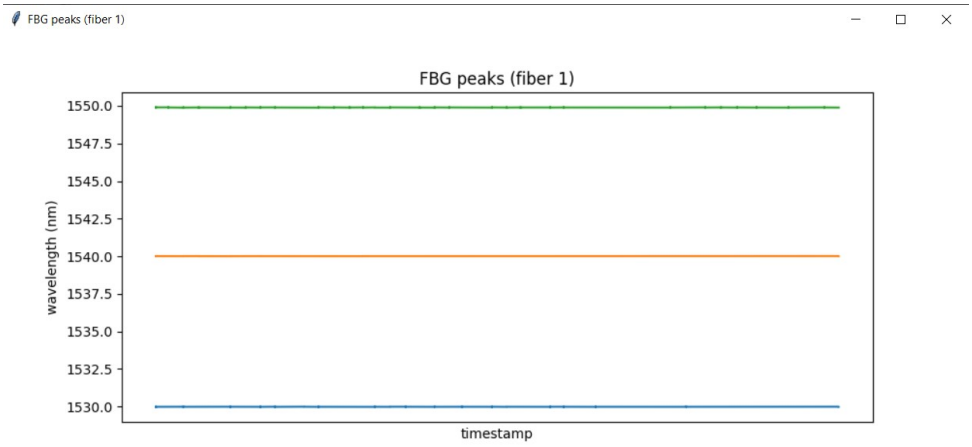

Figure 4.2: Plot obtained from GUI of Peaks vs Timestamp

- **Fiber Status**: This is a small functionality set in the GUI that shows the the fiber that is connected and how many sensors does the fiber consists by calculating the number of peaks obtained in the sample data for each fibers. This can also be used to verify and validate the threshold value or the sensitivity of the interrogator during the capture process.

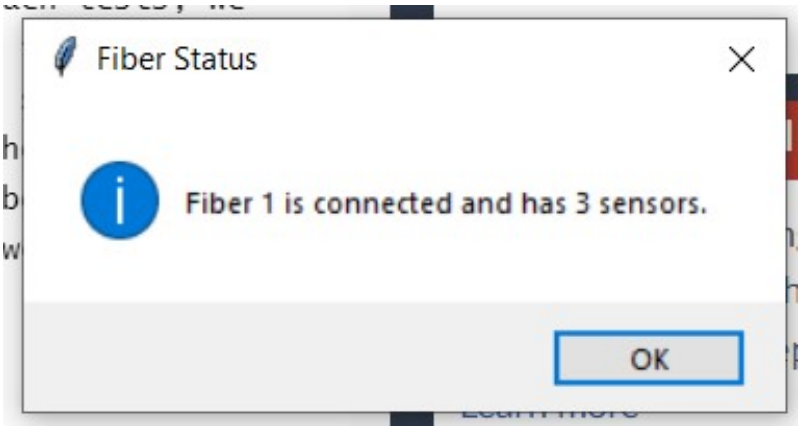

Figure 4.3: Fiber status of GUI

- **Save Data**: To save the obtained sample data (insert reference), this function can be clicked once the capture process is completed and successful, and the obtained sensor data can be saved in CSV format at user-preferred location.

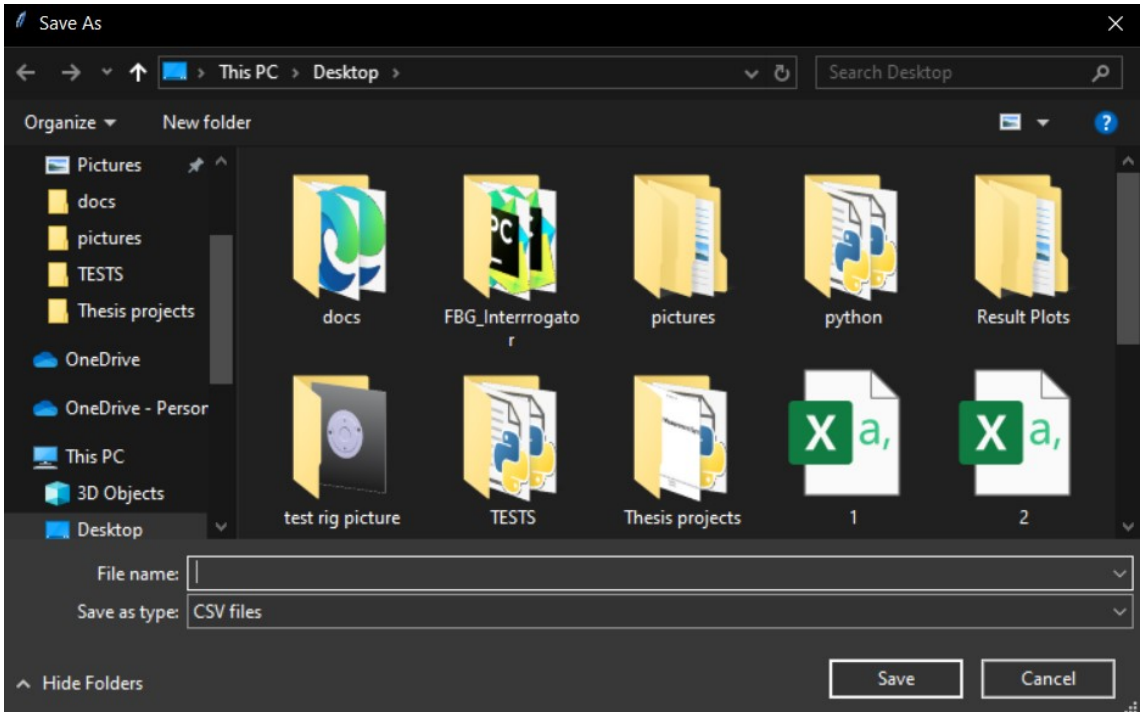

Figure 4.4: Save as CSV format from GUI

4.2 Post-processing results

From section 3.4 and fig 3.17, it can be seen that the data for samples are alternating between the two fibers. To work on the data, it had to be separated based on their fiber ids, and this is how it looks after.

	timestamp	fiber_id	peak1	peak2	peak3	peak4	peak5	peak6	peak7	peak8	peak9
1	2024-05-14 13:54:31.237023	1	1512.577255	1517.450521	1528.953177	1533.824066	1539.571613	1544.538990	1549.536159	1554.980299	1560.134561
3	2024-05-14 13:54:31.237023	1	1512.578204	1517.452256	1528.953172	1533.824051	1539.571599	1544.539009	1549.536208	1554.980560	1560.145710
5	2024-05-14 13:54:31.237023	1	1512.577709	1517.450843	1528.953190	1533.824021	1539.571601	1544.539110	1549.536143	1554.978837	1560.118378
7	2024-05-14 13:54:31.237023	1	1512.577324	1517.451036	1528.953207	1533.824087	1539.571605	1544.539089	1549.536132	1554.977422	1560.102250
9	2024-05-14 13:54:31.237023	1	1512.576031	1517.452028	1528.953229	1533.824036	1539.571598	1544.538670	1549.536106	1554.974203	1560.102198
...	...	...	...	...	...	...	...	...	...	...	...
8035	2024-05-14 13:54:41.245364	1	1512.577784	1517.451086	1528.953169	1533.824215	1539.571617	1544.538929	1549.536233	1554.984893	1560.125966
8037	2024-05-14 13:54:41.245364	1	1512.578444	1517.451520	1528.953167	1533.824182	1539.571585	1544.539033	1549.536243	1554.985155	1560.149030
8039	2024-05-14 13:54:41.245364	1	1512.578686	1517.453709	1528.953159	1533.824127	1539.571584	1544.539097	1549.536140	1554.984309	1560.155158
8041	2024-05-14 13:54:41.245364	1	1512.580157	1517.452391	1528.953166	1533.824129	1539.571584	1544.539233	1549.536225	1554.982820	1560.127094
8043	2024-05-14 13:54:41.245364	1	1512.580055	1517.454463	1528.953197	1533.823966	1539.571601	1544.539071	1549.536167	1554.980350	1560.114340

Figure 4.5: Samples after separation

From figure 4.5 above, it can be seen that the samples are of only the first fiber for all the sensors. This can also be confirmed from the sample number on the left, where there are alternate numbering.

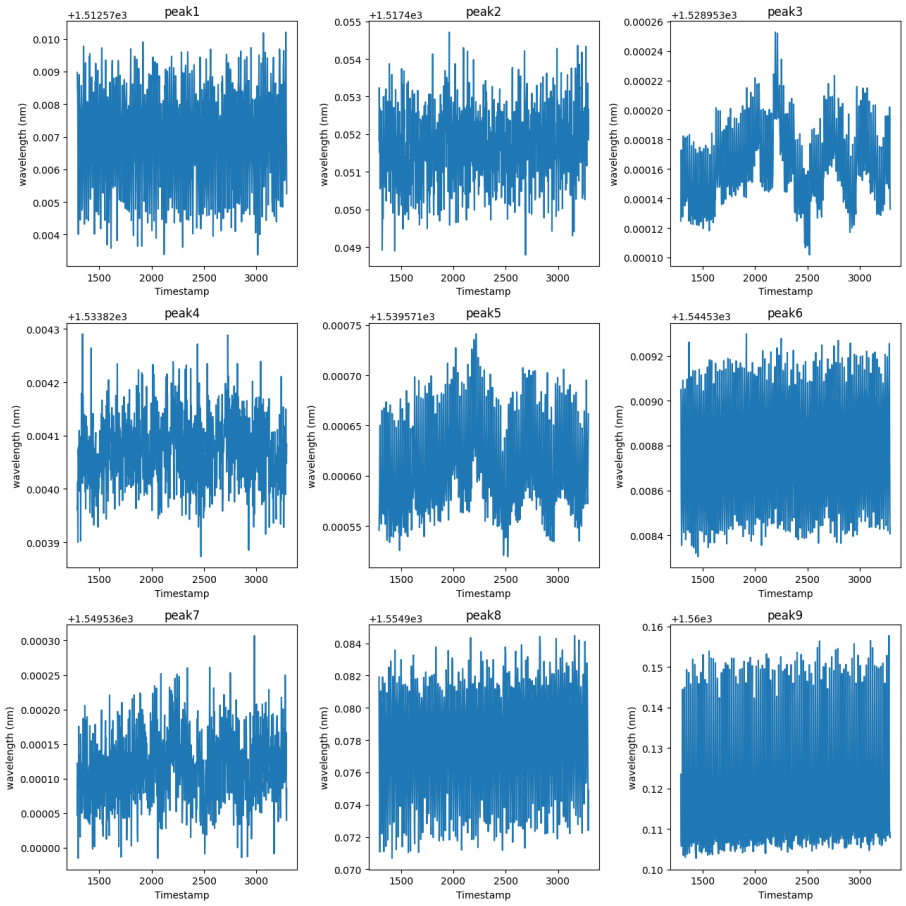

Figure 4.6: Original data for all the peaks

The figure 4.6 above shows us how the data for all the peaks. Here there are 9 peaks where each peaks corresponds to one sensor. We can observe here that, the peaks i.e., data are different and also in different range for different sensors.

4.2.1 Filtered results

For the acquired data after segregation, a function was created to filter out the data using the butter worth filtering. As mentioned in section 3.4, out of the samples we've acquired a random data of 1000 samples were picked every time the function was run and it was filtered for all the peaks. For the filter function, the sampling frequency was set to 400Hz and the order was set to 4 with the cut-off frequency set to 0.125 times the sampling frequency. The images below represents the filtered vs original data for all the fibers at 3000N applied force.

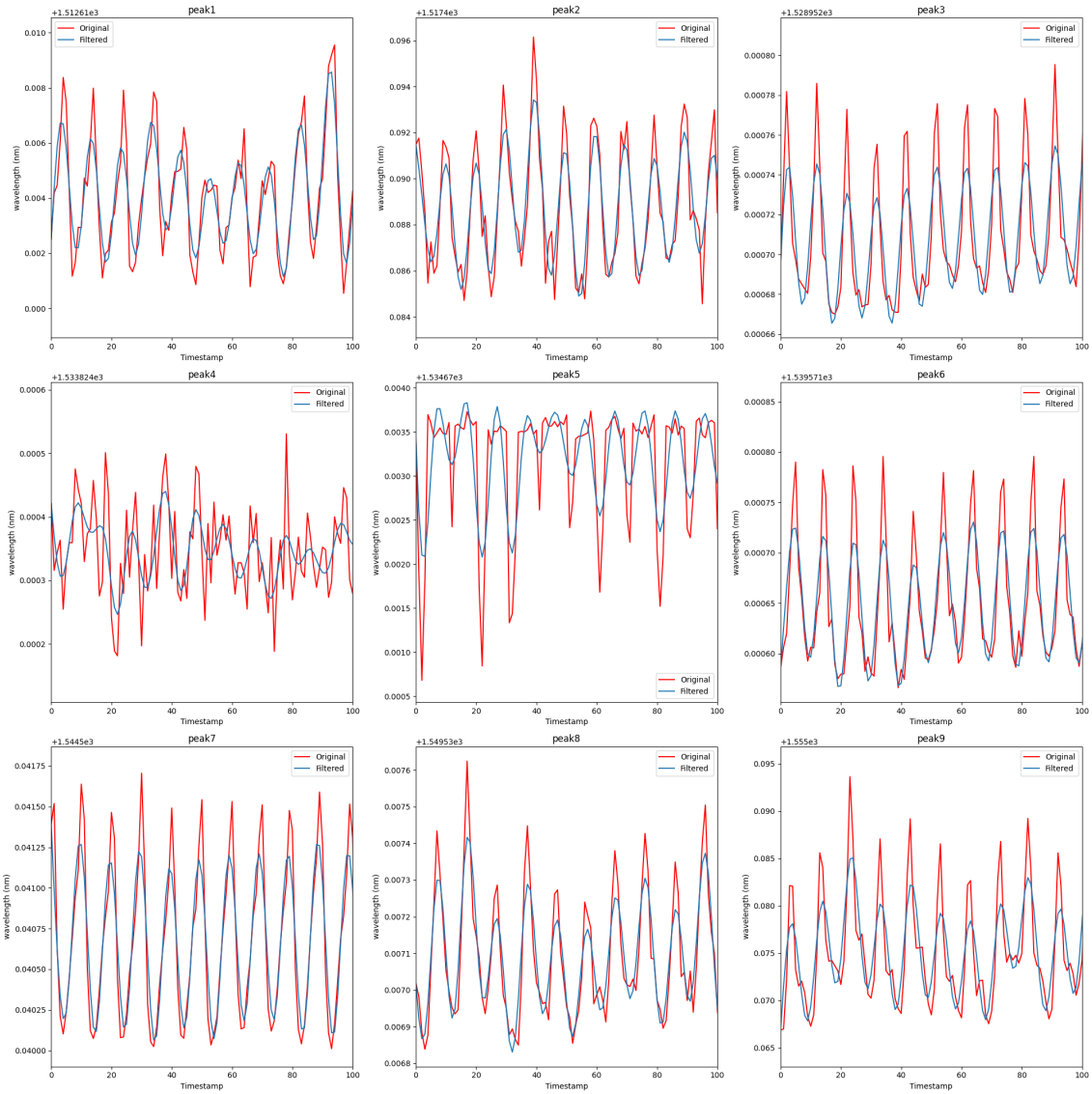

Figure 4.7: Original vs filtered data 3000N for fiber1

Here, from the section of the data was picked at random only 100 samples are plot-

ted. The sinusoidal waves in each peak represents the ball passing that sensor. It can also be seen that sensors 2, 3, 6, and 7 are showing similar trend while 1 and 8 slightly match that trend. Also, sensors 4 and 5 are not outputs as one expects a FBG sensor to give. Despite their position on the bearing i.e., around the bearing and the bearing axis being normal to the ground during tests, we expect all the sensors to give similar results but the plots shows otherwise. The sensor 9 is not considered here because it is exclusively for temperature.

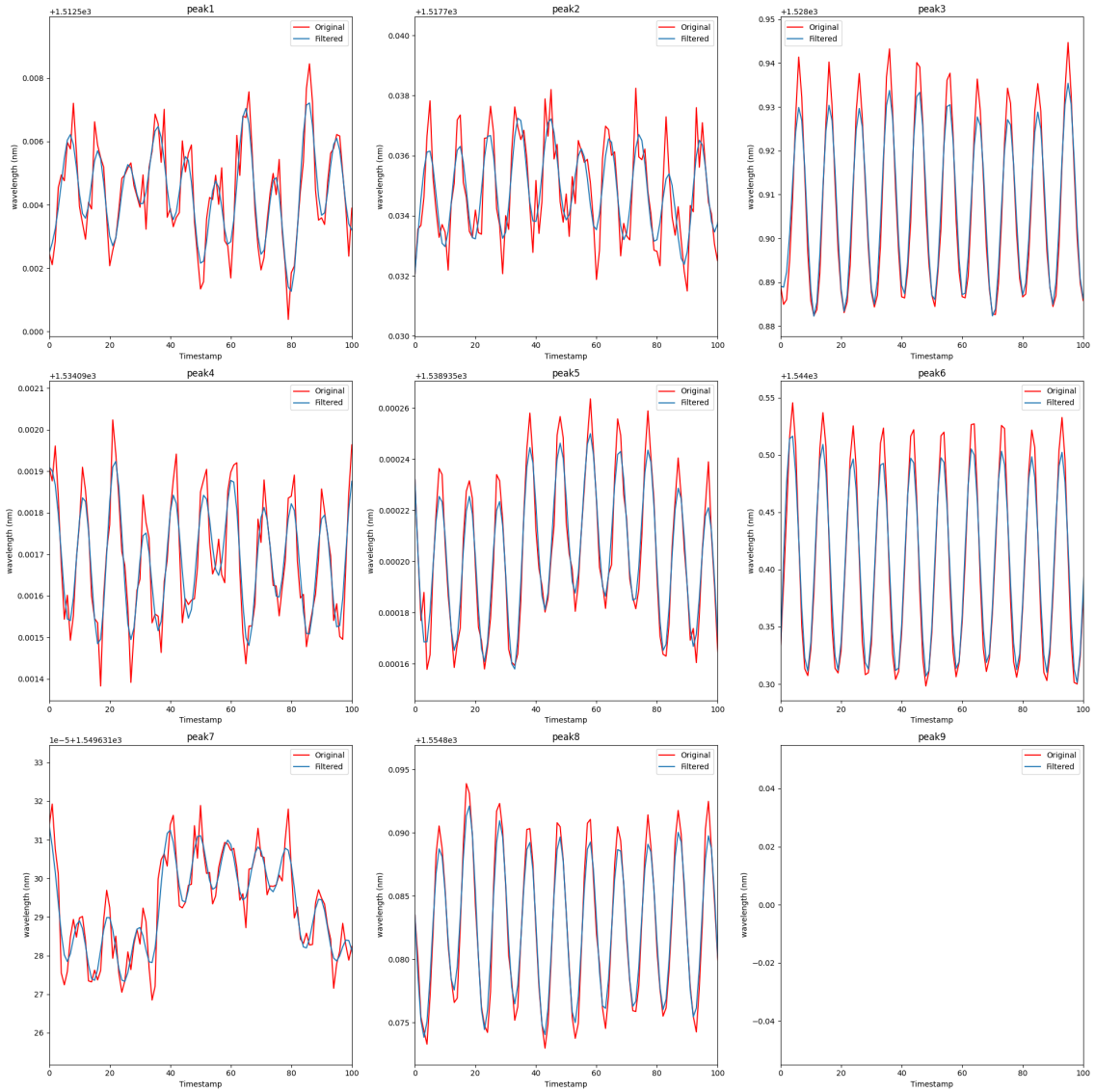

Figure 4.8: Original vs filtered data 3000N for fiber2

From the above figure 4.8 it can be seen that sensor 1 and 7 are behaving completely different than the rest. Sensor 2 and 4 have similar trend and sensors 3, 5, 6 and 8 are similar. Sensor 9 is empty as fiber 2 on driver end has only 8 sensors. It is similar for all the fibers used i.e., two fibers in the drive end and the two in non driving end. For different loading condition, different sensor reacts differently. These results can be seen in Appendix 1 A.

The following plots show the filtered data of all the peaks together starting from the same point.

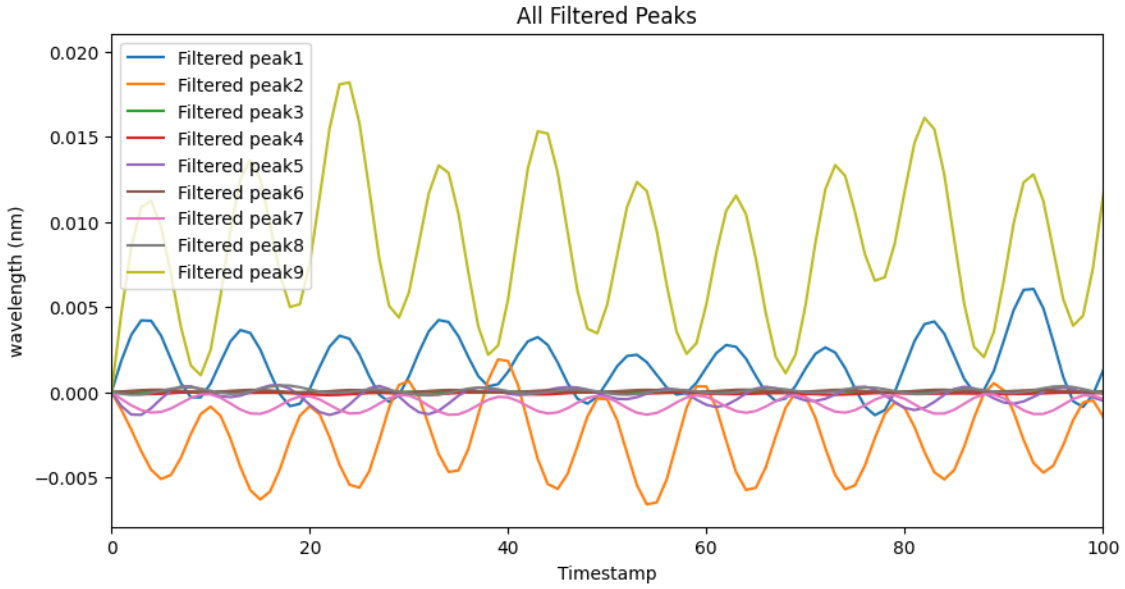

Figure 4.9: All peaks for fiber 1(3000N)

As mentioned above, all the sensors should give out similar results if not the same because of their position in the machine and the way the test is being conducted or can also be a problem of the interrogator we have used. From the filtered figure 4.9 of all the peaks it can clearly be told that the sensors are faulty or they are exposed to other forces apart from the external axial forces applied during the test. The wave amplitude for peaks are very off. Peak 9 can't be considered in this case as it is for temperature measurement purpose whereas the peak1 and peak2 have an amplitude close to 0.005 nm and for peak7 and peak8 it is as low as 0.001. The remaining peaks such as peak3 , peak4, peak5, and peak6 are shown as a strain line. This further proves the fact the sensors being used here are broken or faulty and they might be subjected to different sort of vibrations. Another reason for this might be the problems with hardware resolution of the interrogator. One solution is to up-sample while retrieving the data and check if the results are same. The plots for the other peaks for the same sensor and load can be seen in Appendix 1A including plots for different loads.

4.2.2 Discrete fourier transform

A Discrete Fourier Transform(DFT) is a mathematical model similar to that of a continuous fourier transform where the signal is converted from time domain to frequency domain. According to [19] it can be defined as a sequence of converting N complex numbers x(0) .....x(N-1) to a new sequence of complex number by:

$$X[k] = \sum_{n=0}^{N-1} x_n e^{-\frac{2\pi i k n}{N}} \tag{4.1}$$

for $0 \leq kN - 1$.

where x_n is the nth sample in time domain and the X[k] is the frequency component of the spectrum. However, for computing the DFT , it can be done very well using the Fast Fourier Transform(FFT) algorithm[19].
For the same sample that has been filtered for all the peaks and fibers, a discrete fourier transform function was written. In python using numpy library we can perform discrete fourier transform and normalize it using the following syntax.

$$\text{dft} = \frac{\text{np.fft.rfft(section\_data[peak\_name])}}{\left(\frac{\text{len(section\_data[peak\_name])}}{2}\right)}$$

The fourier transform for the fiber 1 in drivers end at 3000N is present below. This is again taken for all the peaks in the fiber.

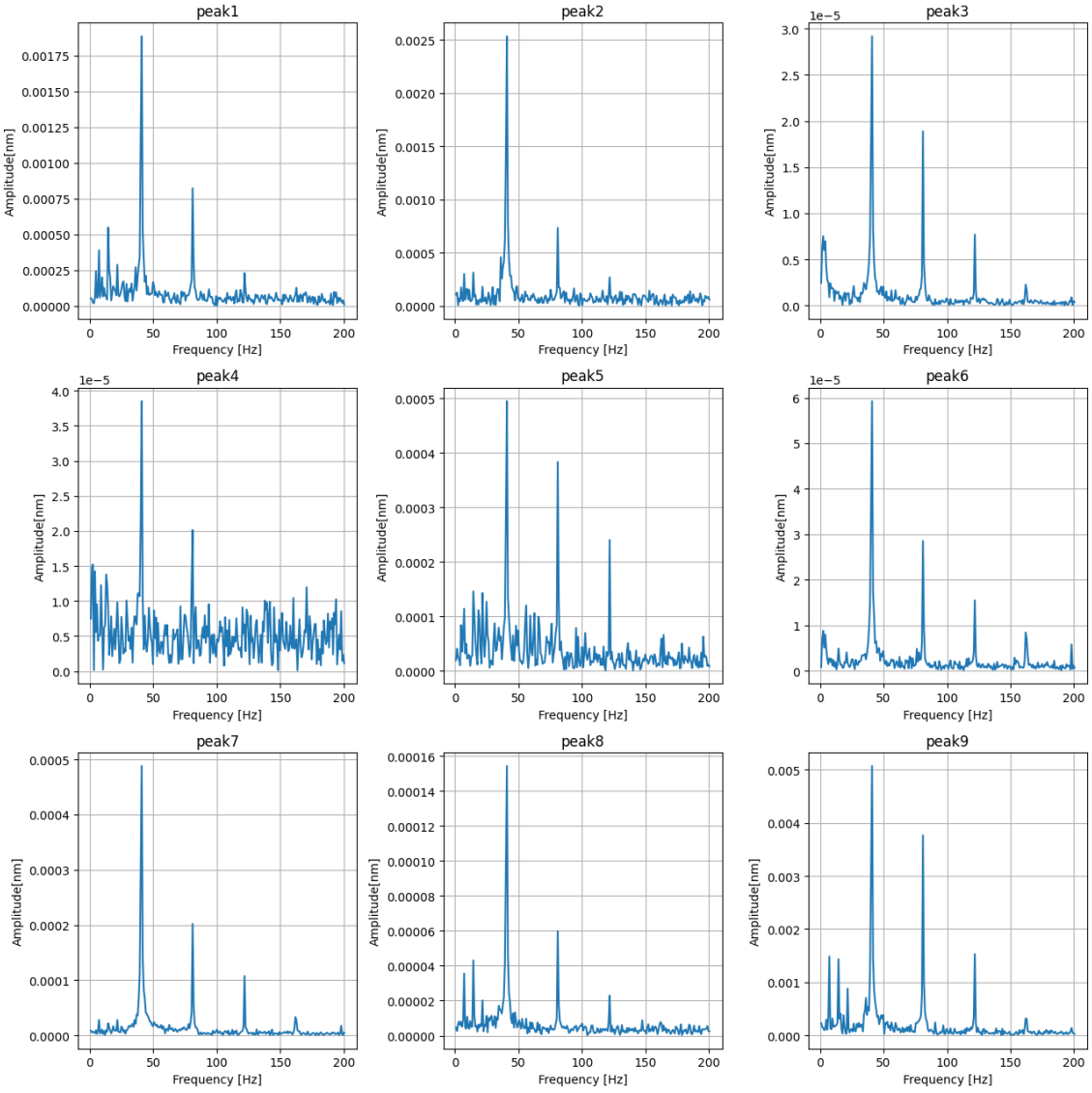

Figure 4.10: FFT for Fiber 1 under an applied load of 3000N

From the plot above, we can see the different frequency components varying with amplitude. The peaks in the plot indicate the dominant frequency where the amplitude is the highest. This frequency signifies the ball pass frequency of the bearing, representing the ball passing over those respective sensors at which the system vibrates strongly.

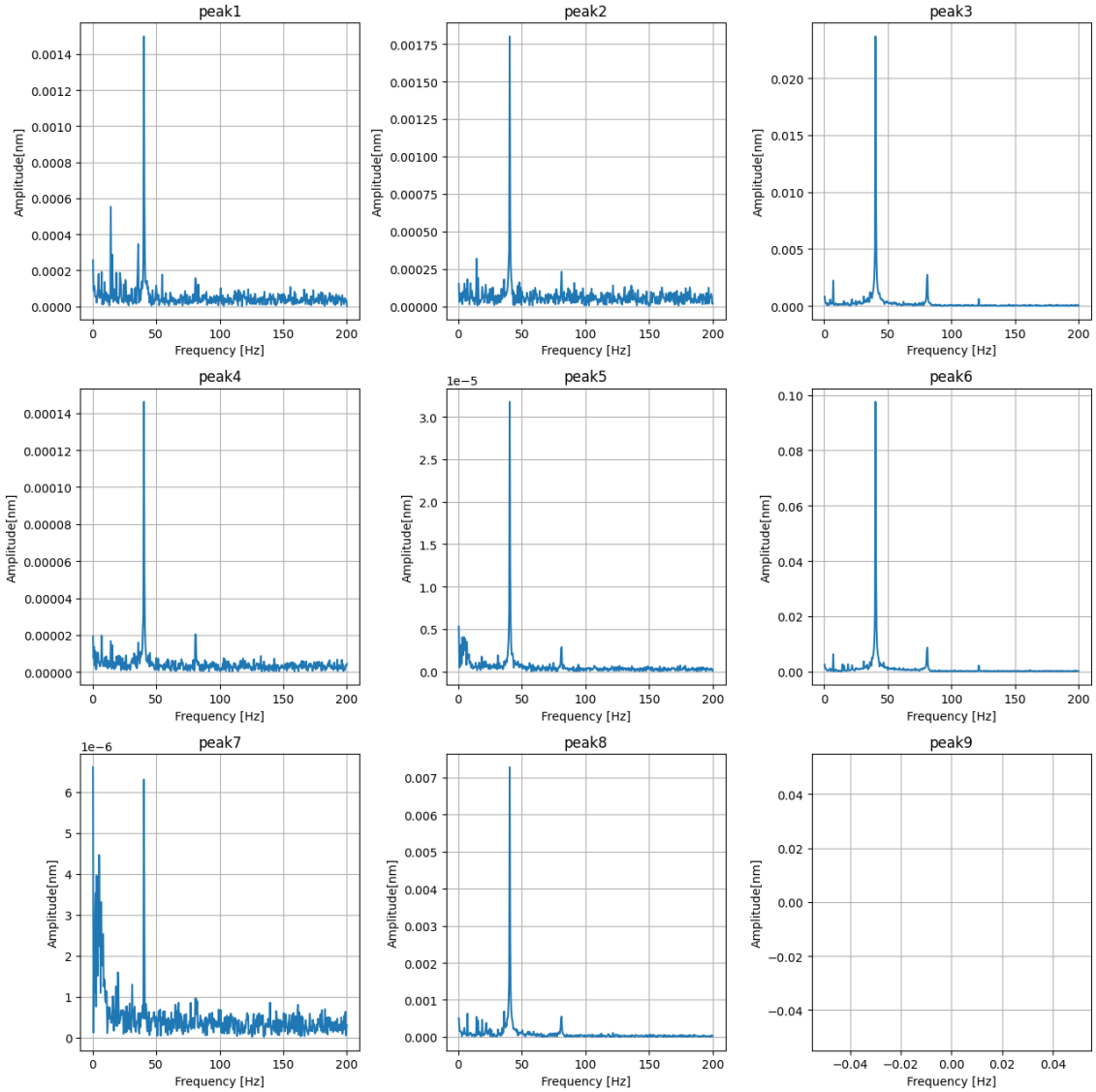

Figure 4.11: FFT for Fiber 2 under an applied load of 3000N

Similarly, you can see the plot of FFT for Fiber 2, which has the same ball pass frequency as that of Fiber 1.
From both plots, we can observe that the frequency at 40Hz corresponds to the ball pass frequency (BPF), indicating that a ball passes the sensor about 40 times per second. The peaks at 80Hz and 120Hz represent the harmonics, which are a result of the periodic nature of the ball pass frequency.
We can also observe disturbances in the sensor readings. The main reasons for this can include environmental noises, such as those from the hand-drill used to rotate

the machine from the driving end, other external vibrations, changes in temperature, and calibration errors of the sensors in terms of misalignment or sensitivity.
Here is a table that represents the RPM of the rotor shaft rotated with a hand-drill and recorded using a tachometer, compared to the RPM of the rotor shaft calculated using the ball pass frequency (BPF) using the equation mentioned in Section 3.4:

Table 4.1: Comparison of RPM values from Tachometer and FFT under different loads

LOAD (N)	**From Tachometer (RPM)**	**From FFT Results (RPM)**
500	446	445.6
1000	439	439.28
1500	436.2	437.14
2500	427.9	438.75
3000	431.6	438.23
4000	424.8	430.71
5000	415	422.1

4.2.3 Relation between Applied Force vs Wavelength shift

There is a certain rise in amplitude at 0 frequency at in the fft plots that has been hidden due to indexing. This rise in amplitude at 0Hz usually represents the average value of the input signal. Using this average value for all the peaks i.e., the average wavelength shifts for all the peaks, it was possible to find a relation between force and average peak. With increase in force, it can be seen that there is a increase in the wavelength shift in the sensors which basically corresponds to the increase in strain. Higher the shift in the wavelength, higher is the strain experienced.

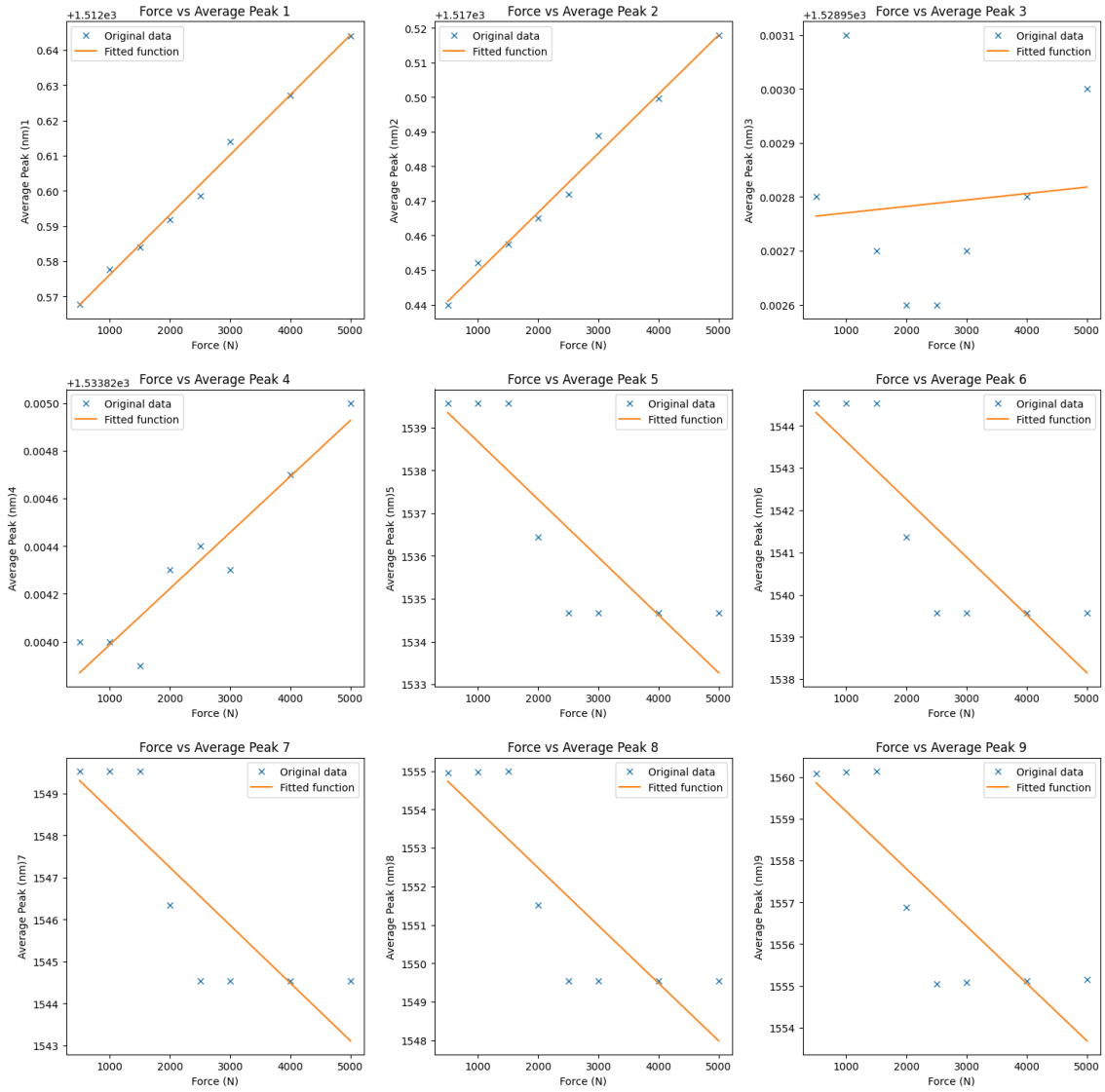

Figure 4.12: Force v/s Average peaks for Fiber 1

Theoretically, as applied force increases, the strain should increase. However, we observe in this plot that not all sensors exhibit this exact phenomenon. Based on the linearity of the fitted function, we can infer that Sensor 1 and Sensor 2 out of 8 sensors of fiber 1 are working as expected, whereas the rest are dysfunctional. Although there is a linear increase in Peak 4, the values of the wavelength indicate

that the sensitivity and accuracy of this sensor are poor, making it non-functional. Similarly, here is the plot for Fiber 2:

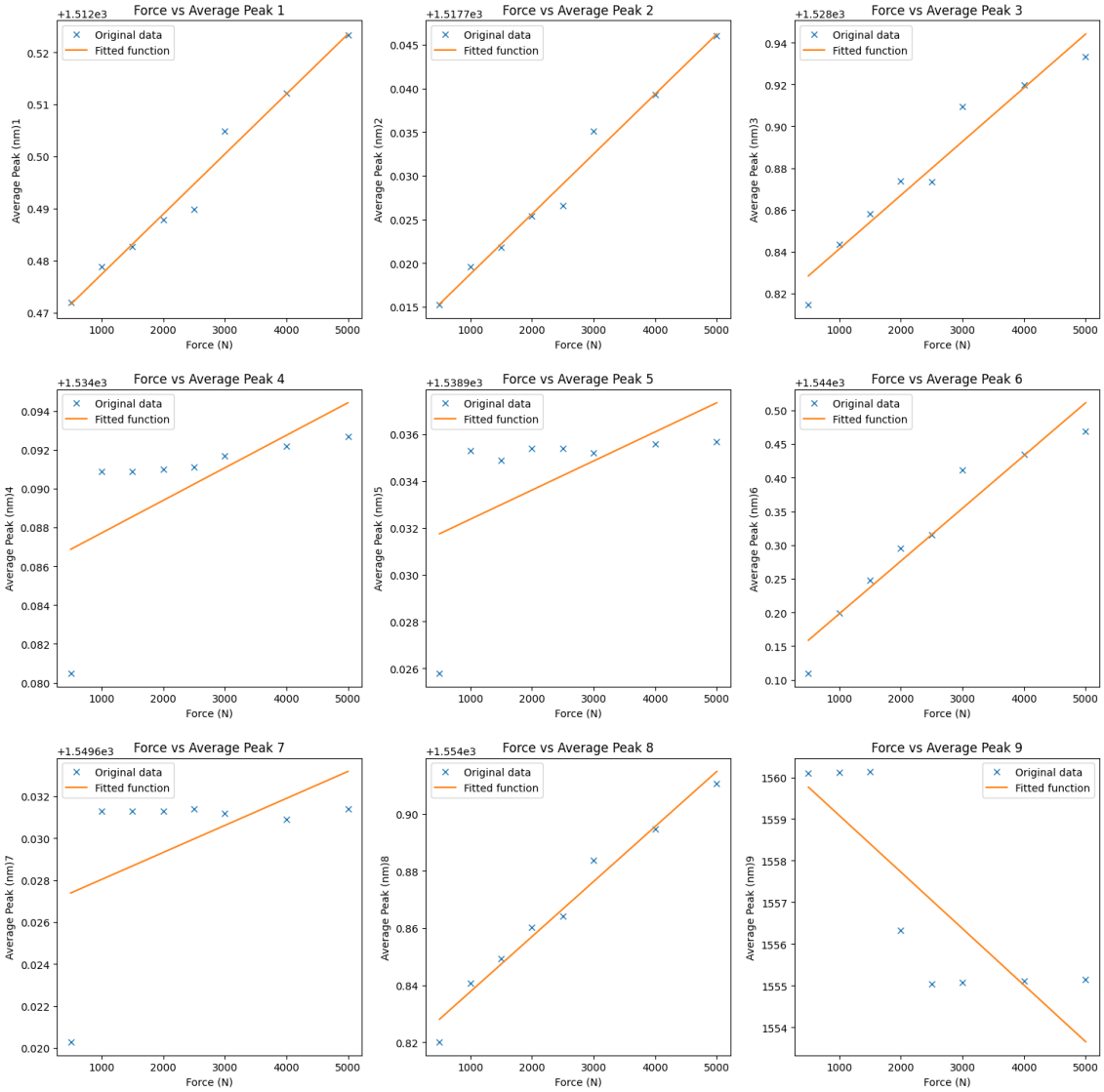

Figure 4.13: Force v/s Average peaks of Fiber 2

From this, we can conclude that Sensors 1, 3, and 8 of fiber 2 are the only ones functioning correctly showing a linear relationship. Others is deemed non-functional due to poor sensitivity and accuracy based on its weird results obtained for each forces.

5
Conclusion

This thesis was set to investigate if the Fiber Bragg Grating sensor can be used as measurement system for future testing of the vehicles. From comprehensive literature surveys, experiments, and data analysis the investigation has given some key findings. With only a few good sensors out the 8 sensors in each of the fibers, the results from these sensors have been quite promising. The axial test experiments over various loads, was able to validate the effectiveness of these sensors. Despite most of the sensors not functioning as expected, it was still possible to determine the ball pass frequency in the bearing from those sensors. It was also possible to determine the relation between the force and the wavelength shift from the good sensors. With increase in the force, the wavelength shift increases meaning the strain increases.

In addition to that, the GUI developed by us has proven to be working very effective and efficient in capturing, storing and visualising the data. This GUI can be used with this interrogator model for any type of FBG tests and is not just limited to this particular test.

Despite many outliers in the sensors for this thesis, it can be said that with more research, development and testing, these sensors have the potential to be used as a measurement tool or system for future vehicle testing.

In summary, the validation of the sensors for as measurement tool for future vehicle was partly successful and the GUI developed proved to be a very efficient for us. The findings from this thesis can serve as a good foundation for future tests.

6
Future Scope

From the methodology, results and conclusion of this thesis project, we can provide some insights and predict the recommendations for future testing and development, projects and thesis on this FBG sensors.

- **Investigating the reasons for Sensor failure or damage**: Since the test setup we got with the sensors were already integrated to the bearings and we had no control in this matter, we recommend in identifying and mitigating the various reasons of sensor failures, which can include environmental factors such as temperature, vibrations or even unwanted miscellaneous particles that can ruin the sensor functionality.

- **Exploring more ways to integrate the fibers on the bearings**: We believe that there are more innovative ways for theses fibers that can be integrated on the bearings that can provide better sensor readings and precise axial strain values when tested.

- **Conducting more tests under different conditions and varying loads**: To ensure the reliability and accuracy of the FBG sensors, the recommendation is to involve extensive testing under diverse conditions and heavy loads in future projects or testing. This can help with validating the sensor's performance and can help in future designs to withstand real-world challenges.

- **Evaluating the actual performance of the Up-sampling process and Hardware resolution of the Interrogator**: Future research must focus on the performance on up-sampling process used by the Sentea interrogator where they up-sample the sensor data to increase the data resolution which is way less than the specified hardware resolution by Sentea organization. This will ensure minimal noise and a larger dynamic range in the quality of the sensor data. The interrogator we have used is the cheapest one available in the market for monitoring system functionality. But there are good interrogators in the market that are way more expensive, so this recommended method is a good way to go about it to increase its reliability for good data resolutions in the future.

Bibliography

[1] "One year of fbg-based thermo-hygrometers in operation in the cms experiment at cern - scientific figure on researchgate," 2024, accessed: 2024-07-05. [Online]. Available: https://www.researchgate.net/figure/a-Fiber-Bragg-Grating-structure-b-Schematization-of-FBG-coated-relative-humidity_fig1_297684451

[2] Fbg principle. FBGS. [Online]. Available: https://fbgs.com/technology/fbg-principle/

[3] I. Boldea, L. N. Tutelea, L. Parsa, and D. Dorrell, "Automotive electric propulsion systems with reduced or no permanent magnets: An overview," *IEEE Transactions on Industrial Electronics*, vol. 61, no. 10, pp. 5696–5711, 2014.

[4] [Online]. Available: https://www.pinterest.es/pin/817192294903985157/

[5] Rohloff AG. Planetary gear system. Accessed: 2024-07-05. [Online]. Available: https://www.rohloff.de/en/experience/technology-in-detail/planetary-gear-system

[6] Sentea, "Product specifications - sentea interrogator," https://sentea.com/interrogator/#product_specs, 2023, accessed: 2023-05-15.

[7] A. Karlsson and E. Marcus, "Evaluation of strain and temperature measurements with fiber bragg grating for loss verification and heat transfer of ball bearings," 2021.

[8] A. Mohammed and S. Djurović, "Electric machine bearing health monitoring and ball fault detection by simultaneous thermo-mechanical fibre optic sensing."

[9] C. A. R. Díaz, C. Leitão, C. A. Marques, C. A. Marques, N. Alberto, M. J. Pontes, A. Frizera, M. R. N. Ribeiro, P. S. B. André, and P. F. C. Antunes, "Low-cost interrogation technique for dynamic measurements with fbg-based devices," *sensors*, 2017.

[10] A. Lamberti, B. D. Pauw, and S. Vanlanduit, "Development of an optical fiber sensor interrogation system for vibration analysis," *Journal of Sensors*, 2016.

[11] [Online]. Available: https://technicasa.com/application/

[12] M. J. Schmid, M. S. Muller, and A. W. Kock, "Fiber beagg grating measurement technology in industry," 2015.

[13] R. Kumar, "Review of electrical machines in electric vehicles," 2023.

[14] E. Agamloh, A. von Jouanne, and A. Yokochi, "An overview of electric machine trends in modern electric vehicles," 2020.

[15] C. Liu, K. T. Chau, C. H. T. Lee, and Z. Song, "A critical review of advanced electric machines and control strategies for electric vehicles," 2021.

[16] W. rapid manufacturing, "Different types of bearings and their characteristics," https://waykenrm.com/blogs/

different-types-of-bearings-and-their-characteristics/, 2021, accessed: 2023-05-27.

[17] C. H. Simmons, D. E. Maguire, and N. Phelps, "35 - bearings and applied technology," in *Manual of Engineering Drawing (Fifth Edition)*, fifth edition ed., C. H. Simmons, D. E. Maguire, and N. Phelps, Eds. Oxford: Butterworth-Heinemann, 2020, pp. 519–545. [Online]. Available: https://www.sciencedirect.com/science/article/pii/B9780128184820000359

[18] J. Corporation, "Jtekt ball bearings: Engineering and innovations," Online, 2023, accessed on 2023-05-10. [Online]. Available: https://www.jtekt.co.jp/e/products/bearing.html

[19] P. Corn, E. Ross, and J. Khim. Discrete fourier transform. Accessed: 2024-07-09. [Online]. Available: https://brilliant.org/wiki/discrete-fourier-transform/

A

Appendix 1

The following figures are filtered plots for different loads on the driving end side.

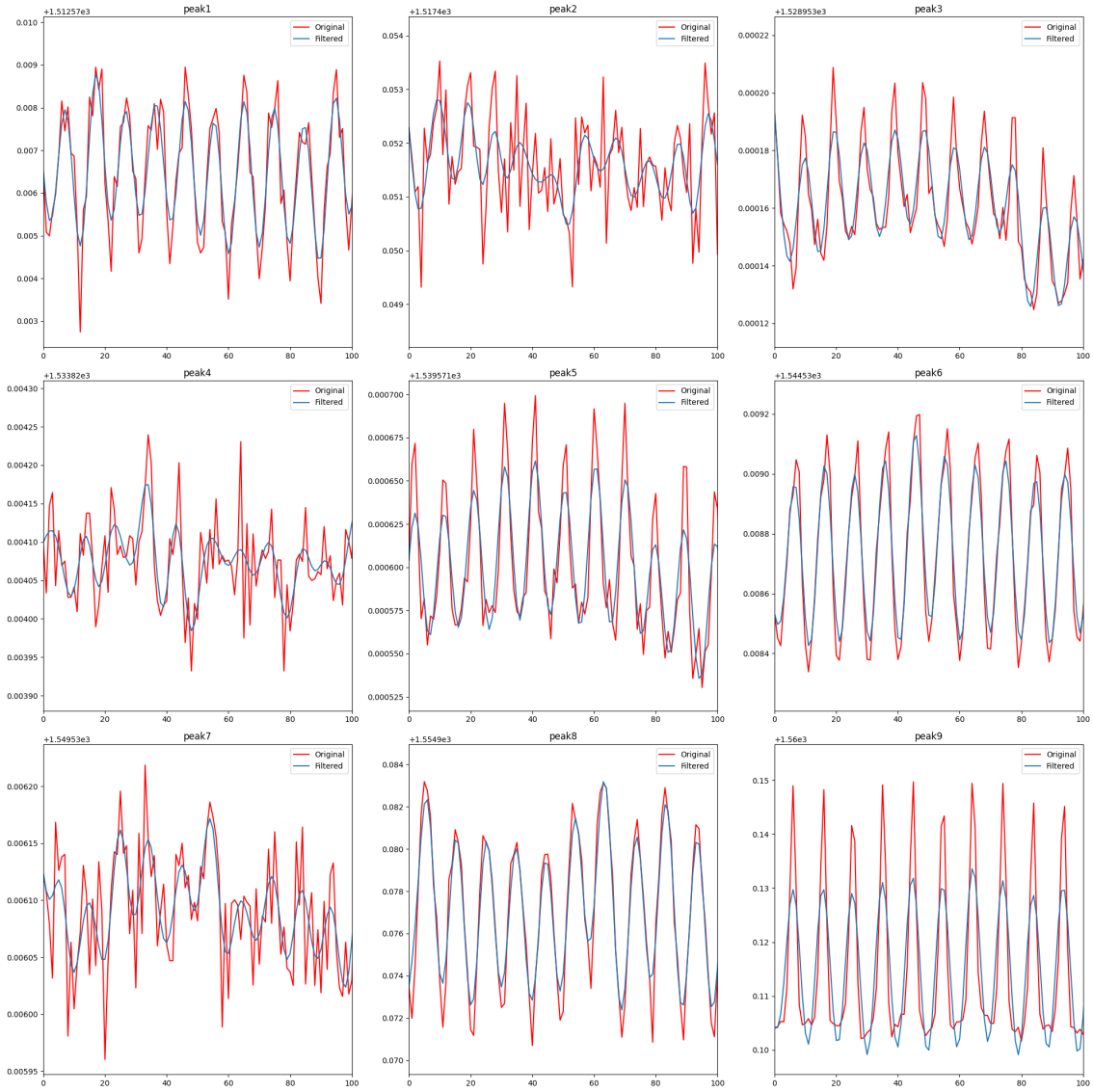

Figure A.1: 1000N fiber1 filtered

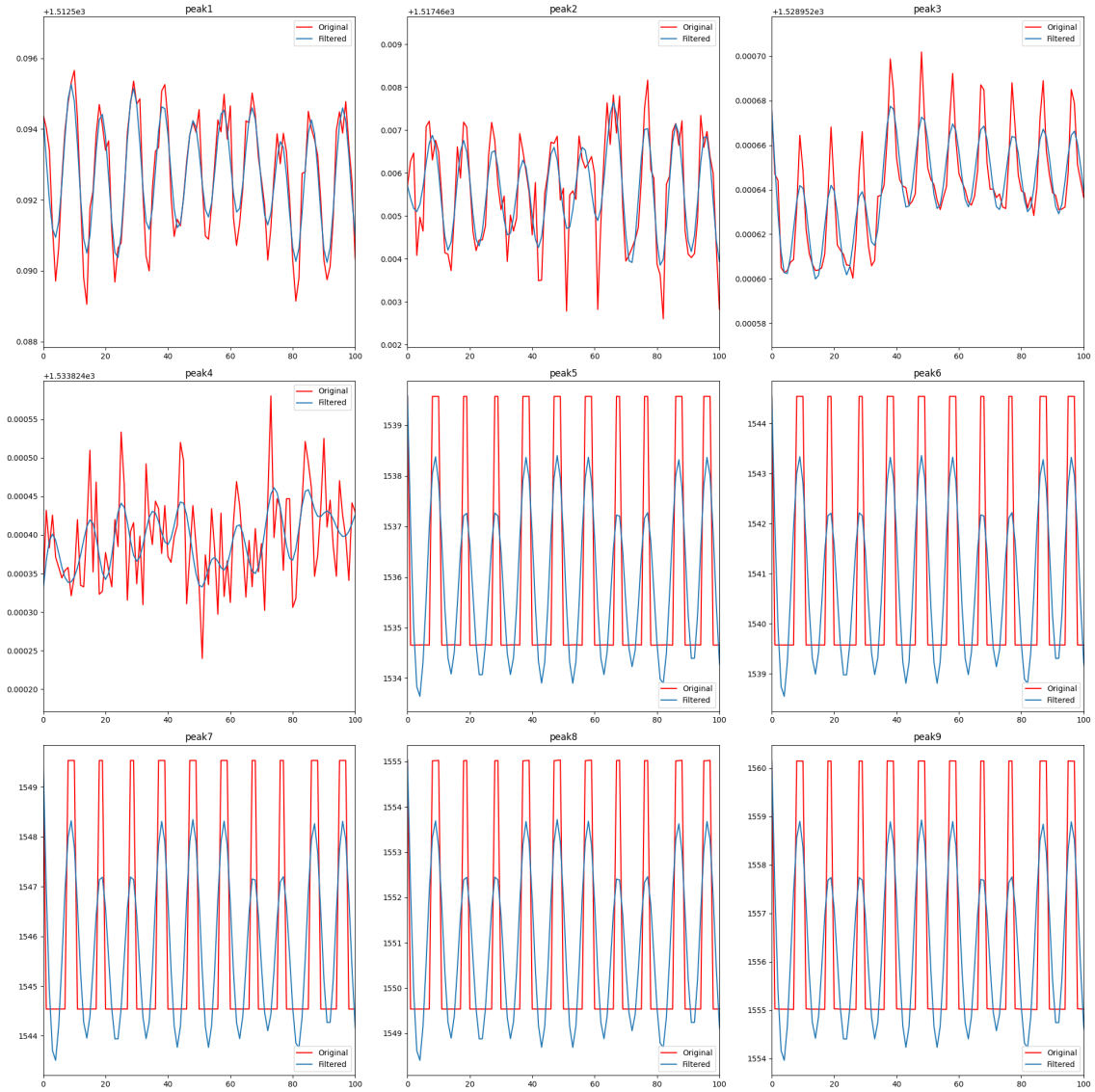

Figure A.2: 2000N fiber1 filtered

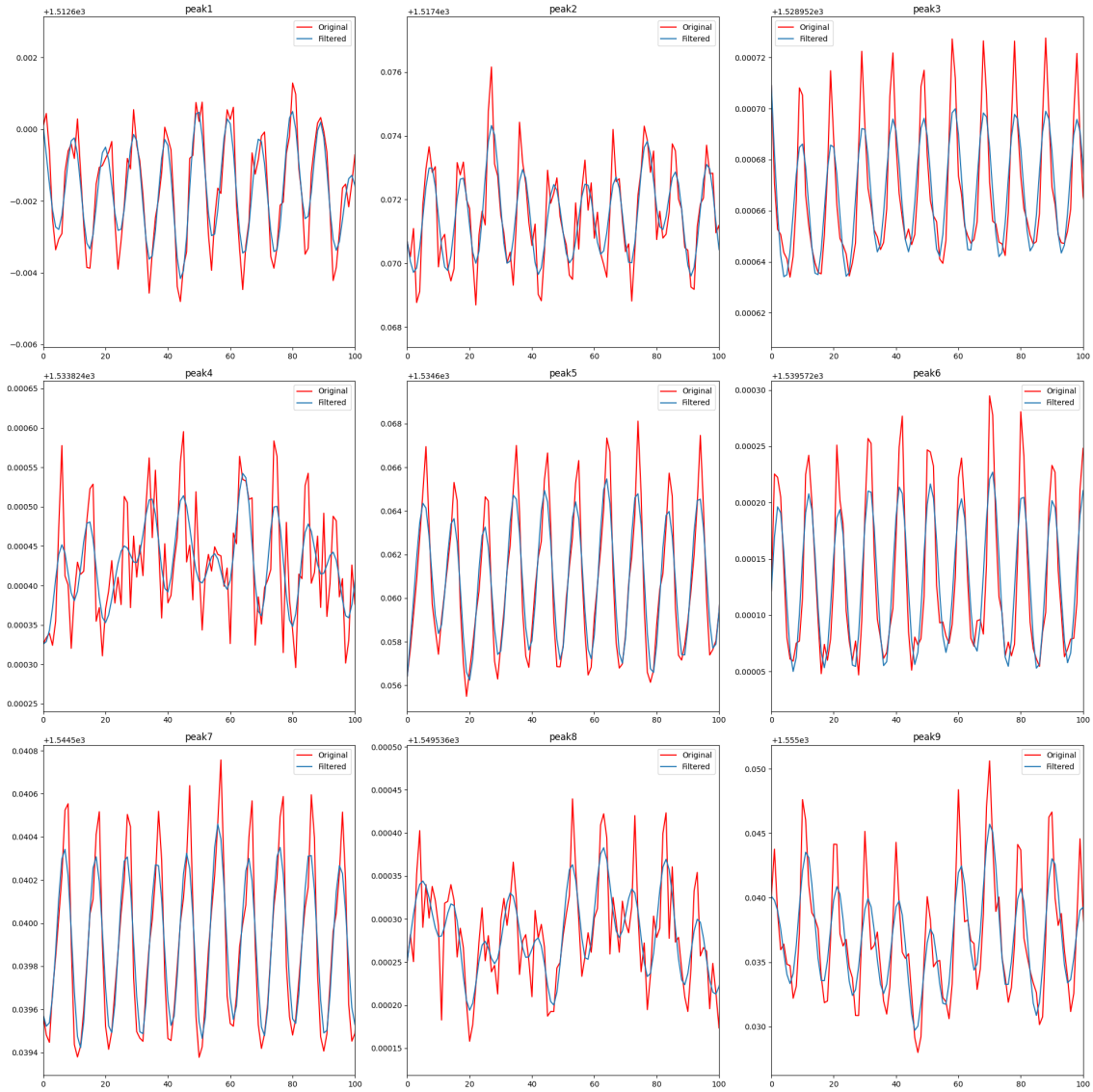

Figure A.3: 2500N fiber1 filtered

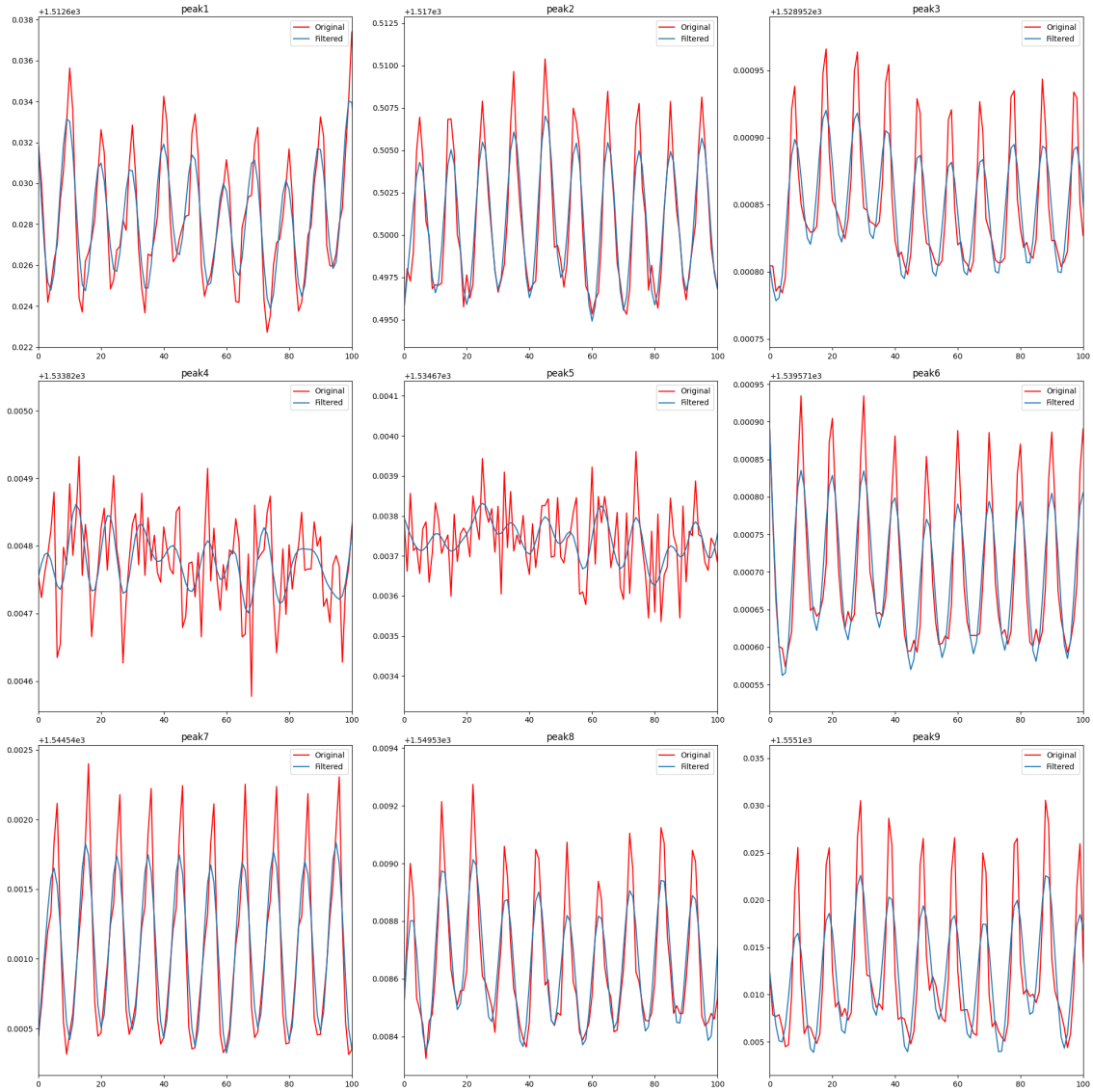

Figure A.4: 4000N fiber1 filtered

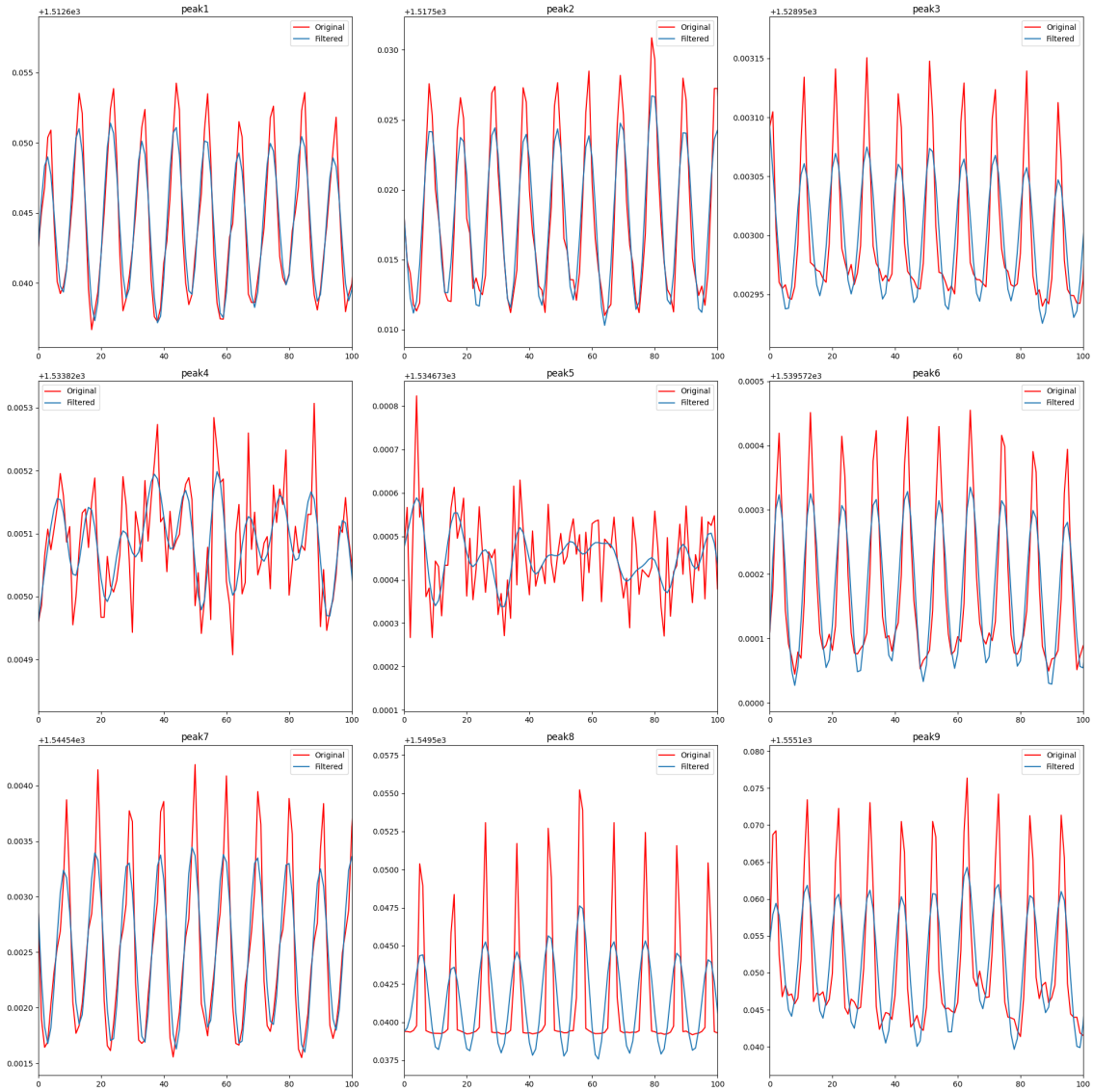

Figure A.5: 5000N fiber1 filtered

The following figures are the plots of peaks of a fiber starting from the same point at different loads. The following plot is in relation to the figure 4.9 where all the

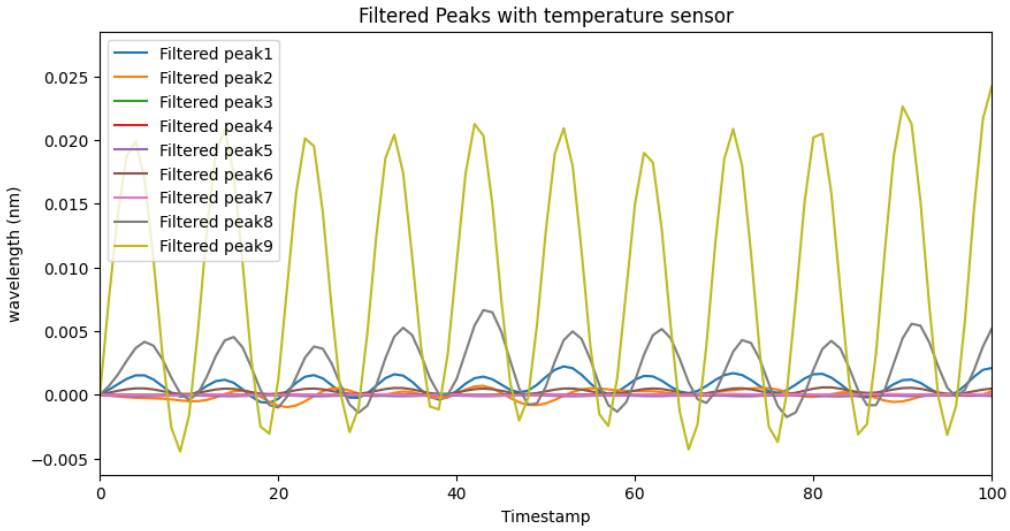

Figure A.6: 500N DE all peaks

peaks of the fiber was plot whereas the peaks plot in figure A.7 are straight line that appears in 4.9.

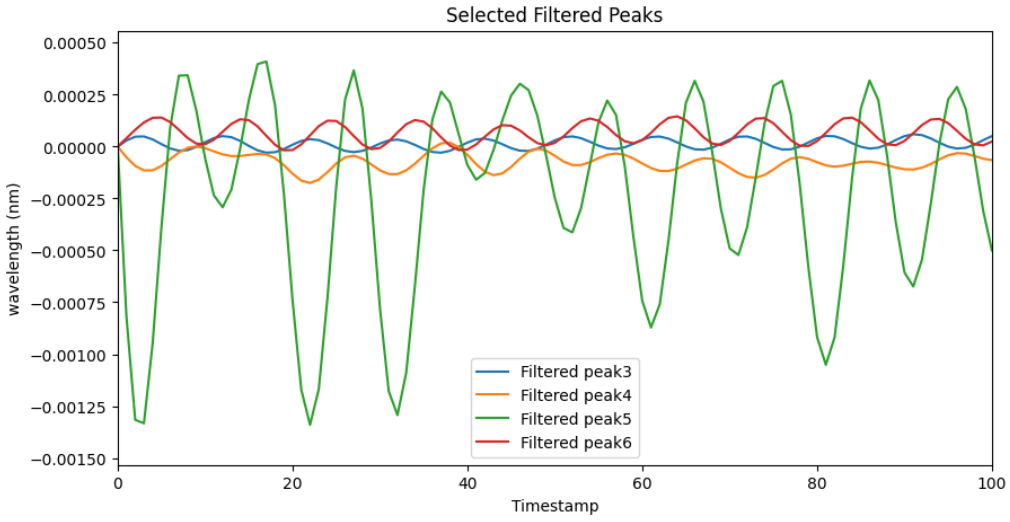

Figure A.7: 3000N DE selected peaks

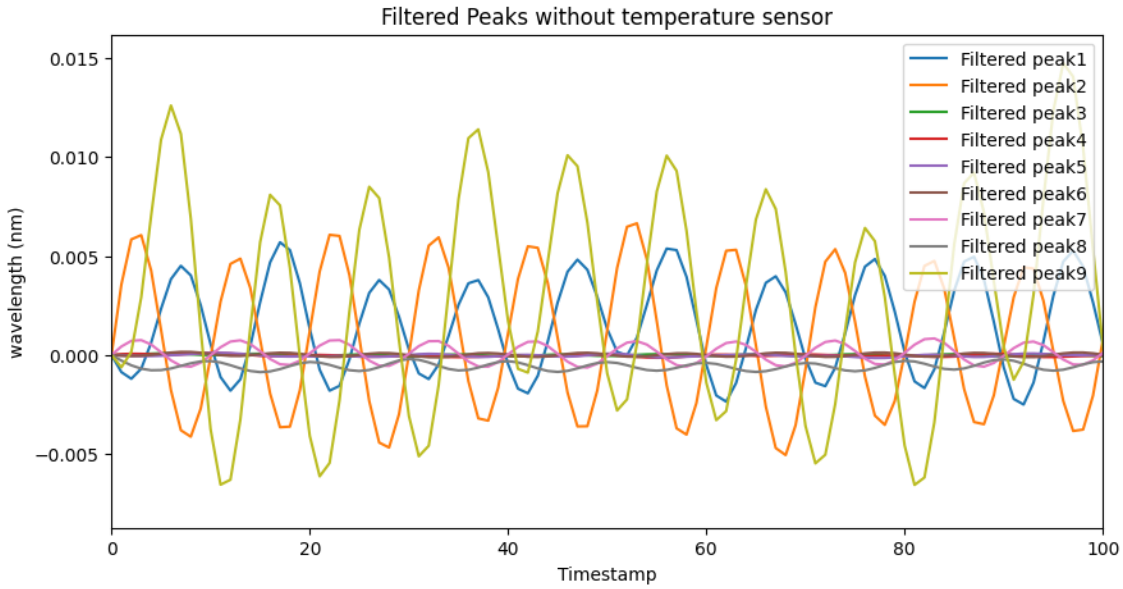

(a) 4000N all peaks

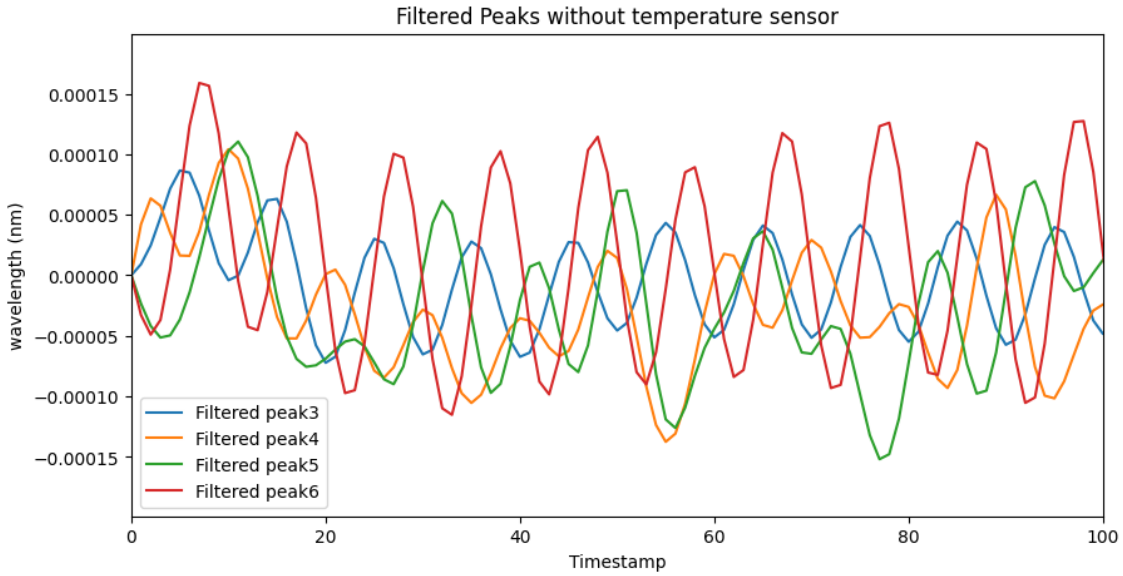

(b) 4000N selected peaks

Figure A.8: 4000N peaks

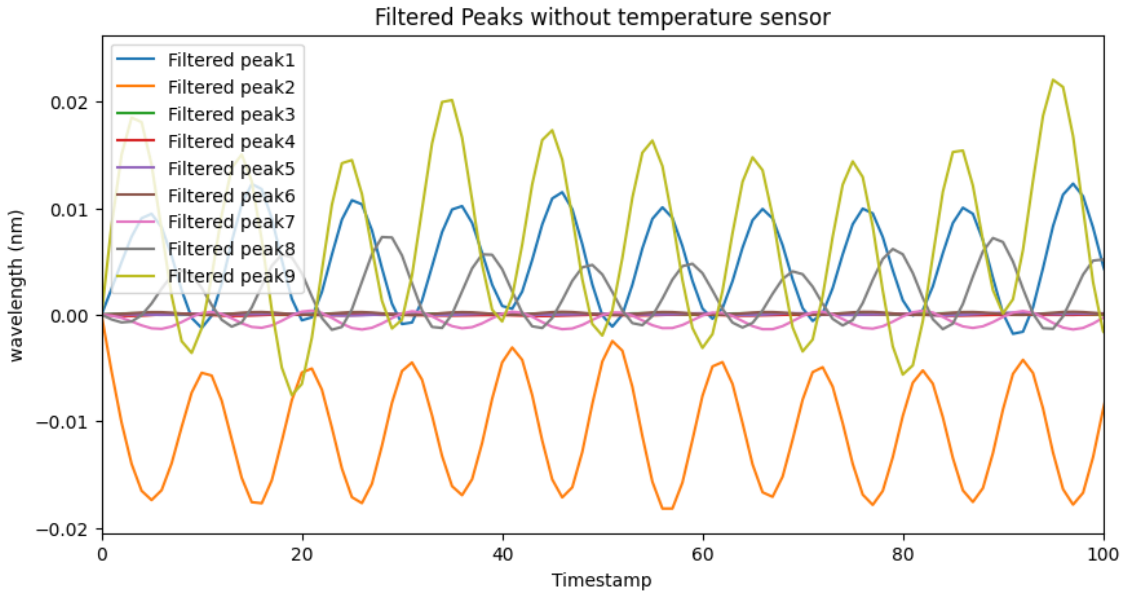

(a) 5000N all peaks

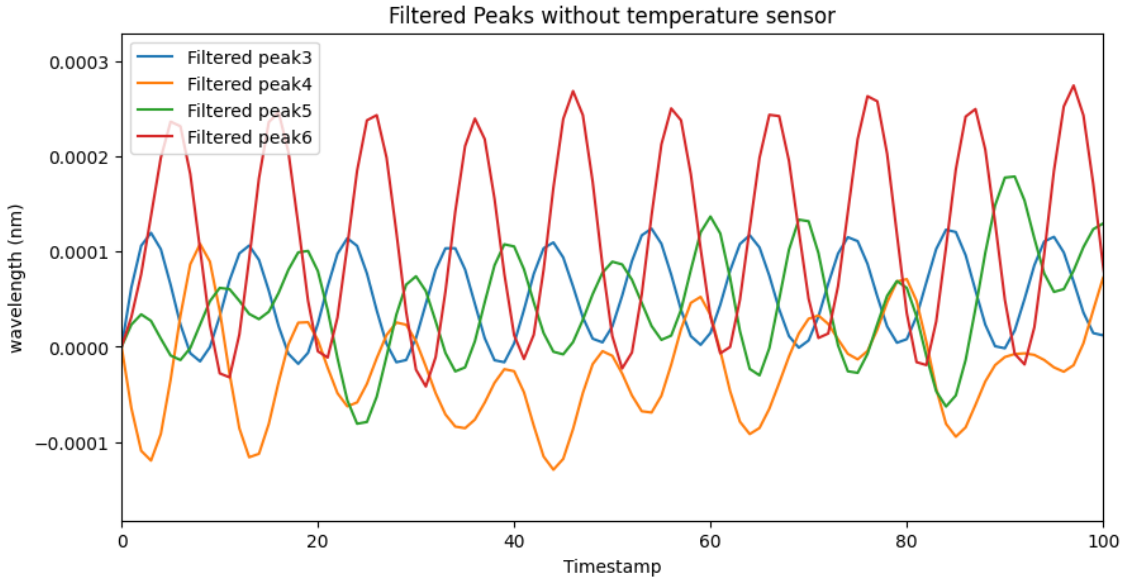

(b) 5000N selected peaks

Figure A.9: 5000N peaks

DEPARTMENT OF INDUSTRIAL AND MATERIAL SCIENCES
CHALMERS UNIVERSITY OF TECHNOLOGY
Gothenburg, Sweden
www.chalmers.se

CHALMERS
UNIVERSITY OF TECHNOLOGY